POLITECNICO DI TORINO

Corso di Laurea Magistrale in Ingegneria Biomedica

Computational modeling of flow in the kidney

Relatore:

Dr.-Ing. Kartik JAIN

Dr.-Ing. Diego GALLO

Prof. Umberto MORBIDUCCI

Prof. Vartan KURTCUOGLU

Candidato:

Claudia BORTOLUSSI

Anno Accademico 2017/2018

Contents

1. Introduction

1.1 Motivation

Kidneys are part of the urinary tract and they are responsible for filtration of blood and production of urine. Kidneys also regulate fluid balance and blood pressure, which are extremely important for homeostasis. The kidneys are the organs of the body that are best perfused in spite of their weight. However, the oxygenation of the renal parenchyma is very low. In response to this condition in which the tissue is deprived of adequate oxygen supply, called hypoxia, kidneys secrete Erythropoietin (EPO), a glycoprotein cytokine, which stimulates red blood cell production in the bone marrow (erythropoiesis). Malfunction of renal O2 regulation can affect red blood cells mass that can lead to the pathogenesis of chronic kidney disease.

Computational modeling can help researchers in a number of aspects, for example testing of hypothesis, producing new understandings, and interpreting experiments. Furthermore, computational models allow repeatability, ensuring many observations on the same subject, while it is not possible to repeat an experiment of the same system under exactly alike conditions. In order to obtain a computational model, an accurate representation of the vasculature of the kidney is needed and, for this purpose, Synchrotron radiation-based technique allows high-contrast imaging of vessels that can be performed at very high resolutions, allowing enhanced image resolution and clarity.

Kidney contains macro and microvasculature. Blood is supplied to each kidney by a single renal artery (that enters the kidney at the hilum and divides in segmental, interlobar, arcuate and interlobular arteries), while venous blood is returned through a series of vessels that corresponds generally to the arterial pathways. The renal microcirculation consists of two capillary beds (glomerular capillaries and peritubular capillaries) that are connected in series by the efferent arteriole and have distinct hemodynamic properties. It is not yet possible to explicitly model both the macro and microvascular networks. For this reason a 1D-3D coupling is employed in order to model the macrovasculature as a 1D network, embedded in a 3D porous media that represents the homogeneous tissue.

1.2 Structure of the Thesis

Following this introductory comments, the second chapter gives a brief view of the renal anatomy. It is followed by the third chapter on the renal physiology, giving a particular attention to the oxygen consumption in the kidney.

The modeling concepts are described in chapter 4, giving some basic definitions to understand the mathematical model. Chapter 5 describes the numerical model and its implementation, emphasizing on the vascular tree representation, to data processing and to its implementation on DumuX. The results on the renal vascular tree are shown in chapter 6, preceded by results of simulations conducted on test-case regarding brain, tumor and cardiac vasculature.

The summary and conclusion of the thesis are reported in chapter 7 as well as the future work.

2. Renal Anatomy

The kidneys, together with two ureters, a bladder and a urethra, are part of the urinary tract. The kidneys are bean-shaped organs located outside the peritoneal cavity, in the dorsal part of the abdominal cavity, one on each side of the vertebral column. In particular, the left kidney lies between the 11th thoracic vertebra (T11) and the second lumbar vertebra (L2), while the right kidney is lightly lower than the other one because it lays under the liver, between T12 and L3, as shown in Figure 1 [1].

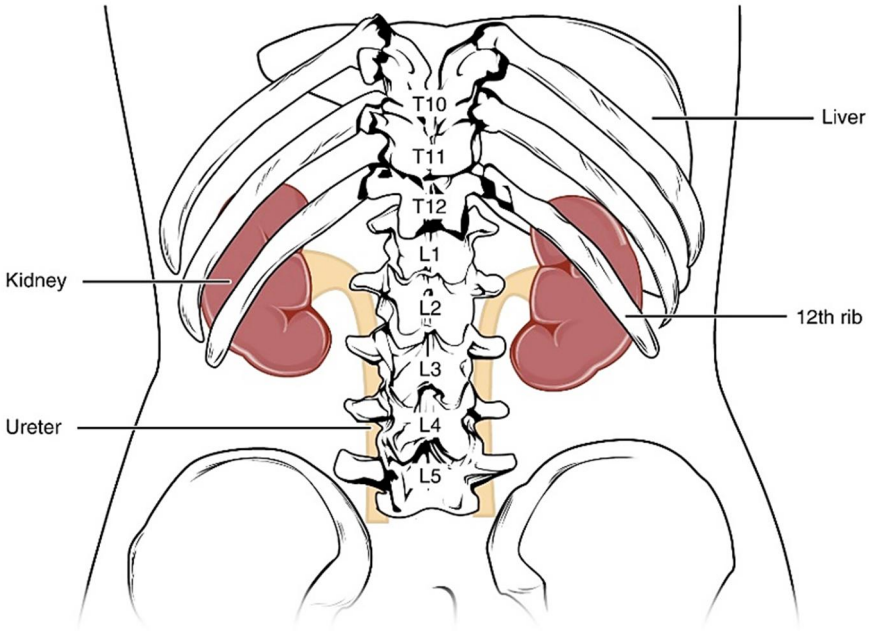

Figure 1: Location of the kidneys
source: http://philschatz.com/anatomy-book/contents/m46429.html

Located just above each kidney are the adrenal glands. Kidneys are embedded in the adipose capsule or perirenal fat, which is a mass of adipose tissue that protects the kidneys from mechanical trauma. The kidneys are held in place by the renal fascia, a collagenous connective tissue that encloses the kidney and the adipose capsule together and locks the kidney to the abdominal wall.

2.1 Structure of the Kidney

The structure of the kidney is well organized and it is adapted for its homeostatic role that execute together the processes of filtration, secretion and reabsorption. Each kidney has a convex external border and an internal border that is concave in the center and convex on both extremities [1].

In the middle of the internal concave border, there is an opening called hilum, through which blood vessels, lymphatics, ureter, and nerves pass to enter or leave the kidney.

Figure 2 shows the longitudinal section of the kidney that presents three main regions, which are from outside to inside the cortex, the medulla and the renal sinus.

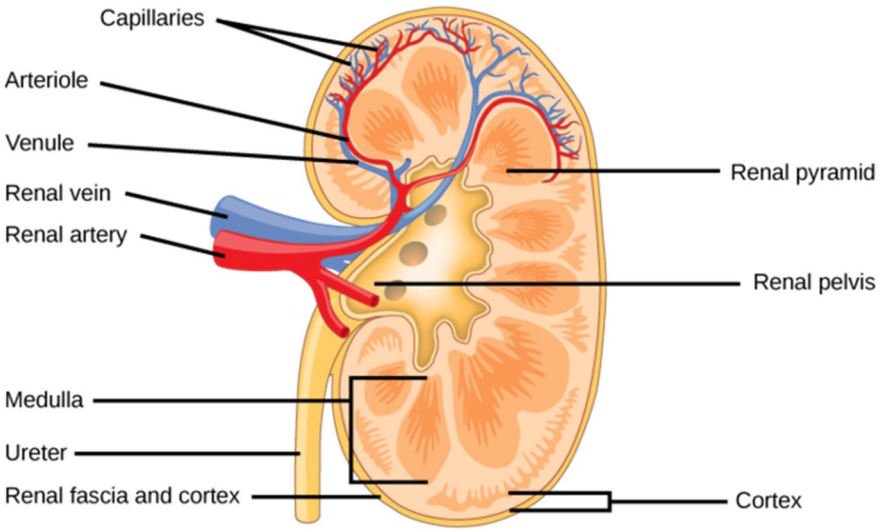

Figure 2: Internal structure of the kidney
source: https://courses.lumenlearning.com/boundless-ap/chapter/the-kidneys/

The cortex and the medulla form together the renal parenchyma and incorporate around a million of nephrons, which are the functional units of the kidney. The cortex comprises two domain: the cortical labyrinth and the medullary rays.

The cortical labyrinth consists of renal corpuscles and convoluted tubules.

The medullary rays contain only straight tubules. These include the initial portion of collecting ducts and portions of varying length of proximal and distal straight tubules of several cortical nephrons. The straight tubules of juxtamedullary nephrons descend directly into the medulla but they do not enter the medullary rays [1]. The structural organization of the renal cortex is shown in Figure 3.

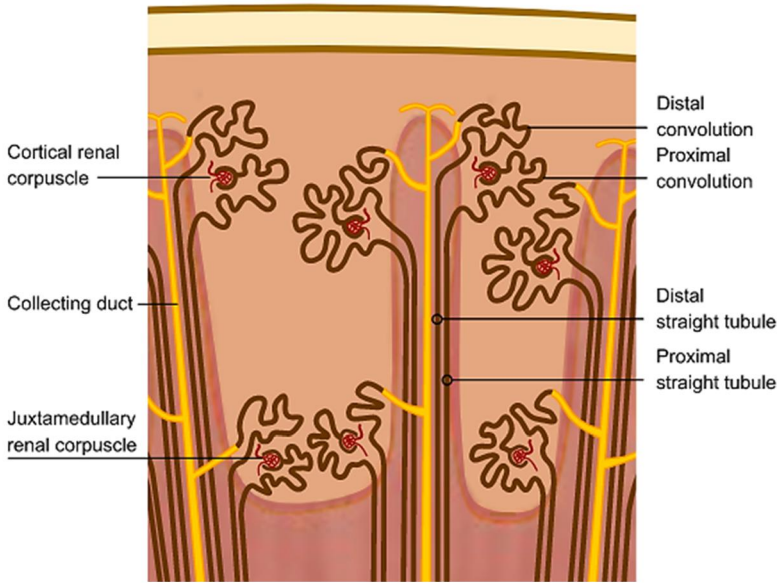

Figure 3: Structural organization of the renal cortex [1]

The medulla can be separated into zones according the distribution of the segments of renal tubules in the pyramid, as shown in Figure 4.

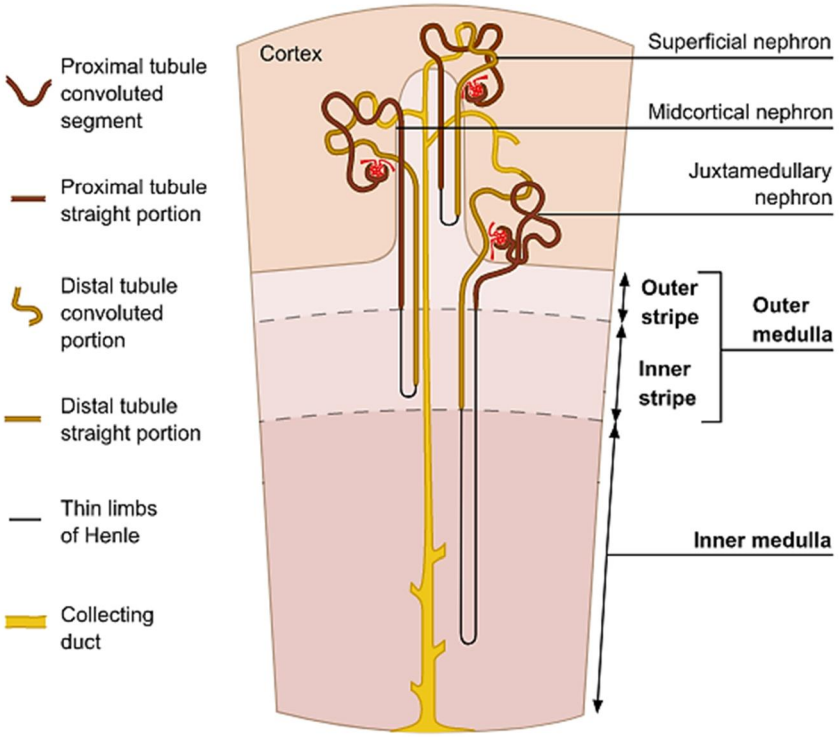

Figure 4: Structural organization of the renal medulla [1]

The outer medulla is proximal to the cortex. It is defined by the presence of profiles of thick and thin tubular segments. Collecting ducts are found all through the renal medulla. The outer medulla is subdivided into outer and inner stripes [1].

The inner medulla is defined by the existence of profiles of thin tubular segments. It contains only the descending and ascending thin limbs of Henle's loop derived from the juxtamedullary nephrons, and the terminal parts of collecting ducts [1].

2.2 Blood Supply

Even though the kidneys compose only 0.5% of the total body mass they are supplied with high amount of blood, and receive over 20% of total cardiac output. The blood is supplied to the kidneys from the renal artery, which subdivides in numerous branches, forming a vascular tree that is responsible for preserving the extremely high perfusion essential for the kidney.

These branches are known as (in descending order): segmental arteries, lobar arteries, interlobar arteries, arcuate arteries, interlobular arteries, and afferent arterioles.

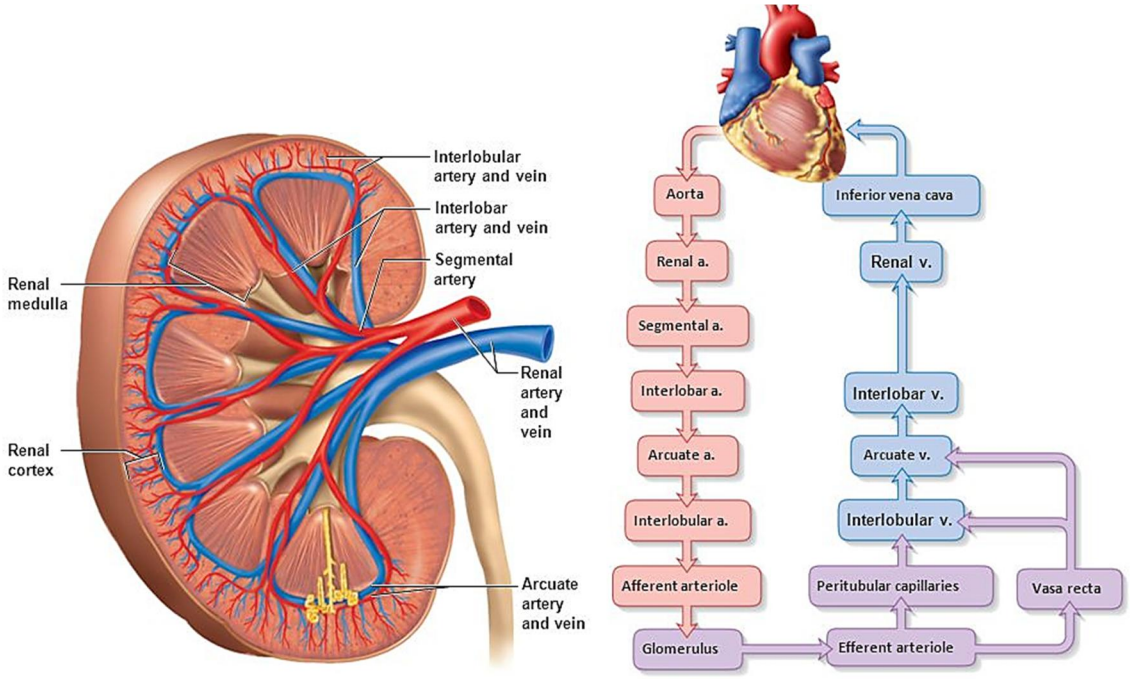

Figure 5: Blood supply diagram
source: http://anatomy-medicine.com/cardiovascular-system/130-blood-filtration-in-the-kidneys.html

The afferent arterioles further splits into capillary networks called glomeruli, which form the beginning of the nephrons. After the filtration process, the blood flows through the network of efferent arterioles that rise to the peritubular capillaries, which supply blood to the cortex and the vasa recta. The vasa recta supply blood to the medulla [1].

Veins they run in parallel to the arteries: blood flows back to the interlobular veins, arcuate veins then back to the interlobar veins, which forms the renal vein that exits the kidney. A summarizing diagram of the renal blood supply is shown in Figure 5.

2.2.1 Renal Microvasculature

The renal microcirculation is composed by two capillary beds that are connected in series by the efferent arteriole and they have different properties. The first is the glomerular capillary bed, which is the area where filtration and formation of primary urine occur, and the second is the peritubular capillary bed, which transports reabsorbed water and solutes back to the systemic circulation. Figure 6 shows the position of both glomerular and peritubular capillary beds and how they are connected between each other. The glomerular capillaries are enclosed between the afferent and the efferent arterioles. This arrangement allows the conservation of a high and relative constant pressure at around 50-60 mmHg inside the glomerular capillaries. This high pressure is responsible for the ultrafiltration of the plasma into the Bowman's space and the formation of primary filtrate [1].

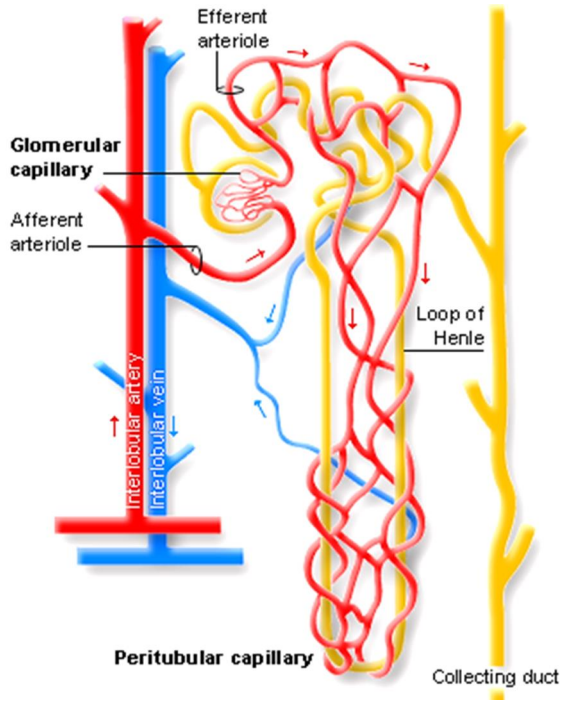

Figure 6: Renal microvasculature [1]

Both peritubular capillaries and vasa recta have comparable properties to other capillary beds in the organism. They are identified by a low pressure system with continuous drop in pressure reaching pressure as low as 5-10 mmHg.

The low hydrostatic pressure in the peritubular capillaries ensure a predominant reabsorptive force responsible for returning the molecules (like water and solutes) absorbed by the tubules from the interstitial fluid to the systemic circulation [1].

2.3 Nephrons

The nephron is the functional unit of the kidney that is responsible for the transformation of the glomerular filtrate to urine. Each nephron is formed by a filtering component, known as renal corpuscle, and a tube specific for reabsorption and secretion, the renal tubule, that extends out from the renal corpuscle and empties into a collecting duct.

The renal corpuscle is an assemblage of the glomerulus and the Bowman's capsule. The glomerulus consists of interconnected capillary loops surrounded by the Bowman's Capsule. The filtrate that exits the glomerulus enters the proximal convoluted tubule, then the loop of Henle. The next segment is the distal convoluted tubule, which opens into the collecting ducts.

The glomeruli of all nephrons are located in the cortical region of the kidney, with the loops of Henle that goes down into the medulla. However, there are two distinct kinds of nephrons: cortical and juxtamedullary, and they are both classified according to the location of their renal corpuscle, as shown in Figure 7.

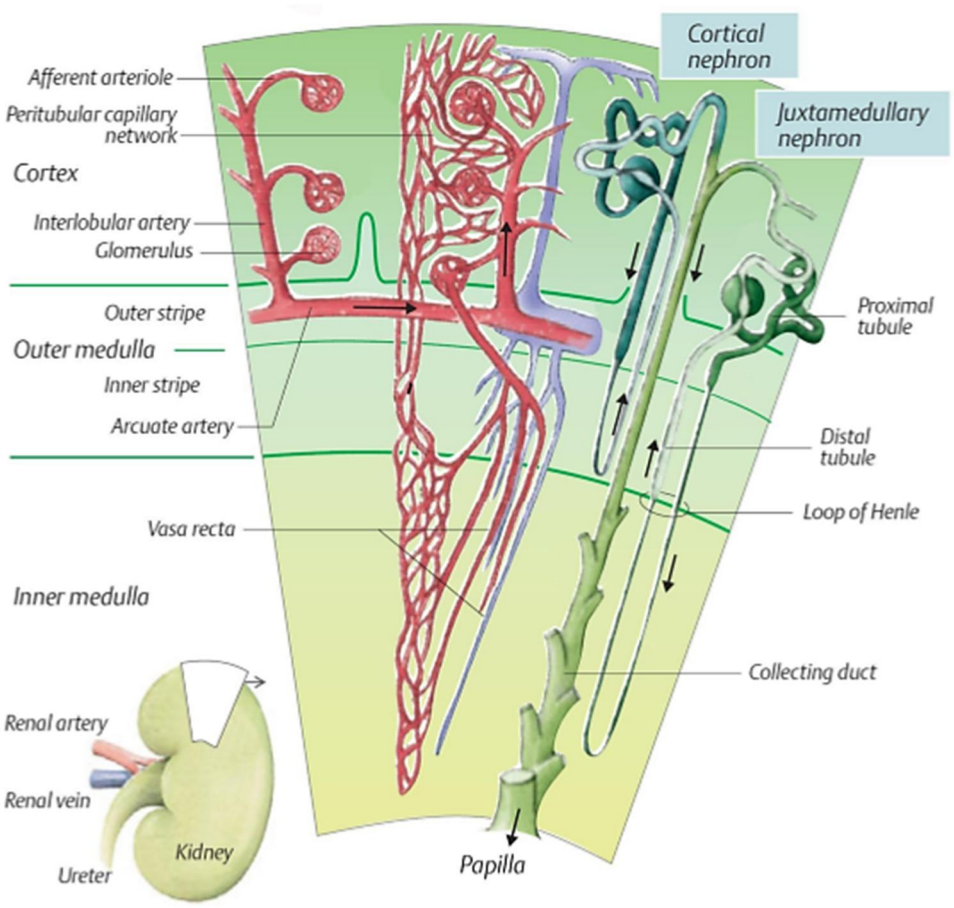

Figure 7: Cross-section of the kidney showing nephron types [2]

2.3.1 The Renal Corpuscle

The renal corpuscle is an irregularly shaped spherical structure where the process of urine formation takes place after filtration of blood plasma. It is formed by the glomerulus, a small network of capillaries enclosed inside a double-walled epithelial cup called Bowman's capsule. Renal corpuscles are located all through the cortical labyrinth of the kidney [1].

The glomerulus is a network of capillaries and it is placed at the vascular pole in Bowman's capsule. Each glomerulus receives blood supply from a renal afferent arteriole. The blood pressure of the glomerulus produces the driving force to filter water and solutes out of the blood plasma, and into the Bowman's space. Only a small part of the plasma is filtered, while the rest flows into an efferent arteriole.

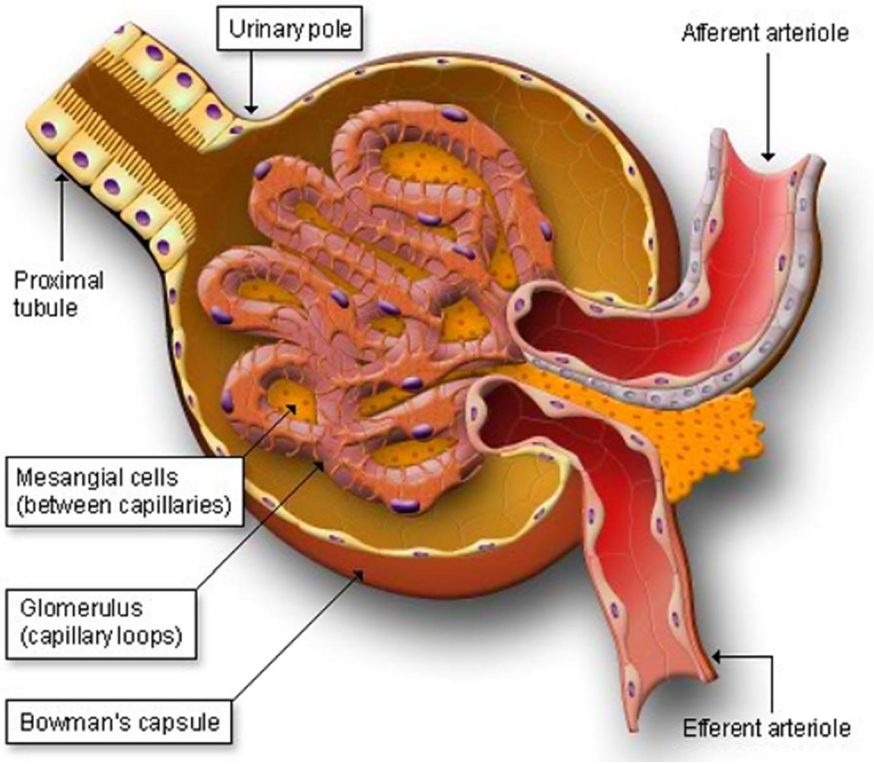

Figure 8: Renal Corpuscle: glomerulus and Bowman's capsule [1]

Bowman's capsule is a sort of cup that collects the filtrate from the blood through the glomerular capillaries. It is composed by visceral and parietal epithelial layers. The space between the visceral and parietal linings is called Bowman's space or urinary space since it collects the filtrate of blood that comes from the glomerular filter. Bowman's space is connceted with the lumen of the proximal convoluted tubule [1]. A representation of the renal corpuscle is shown in Figure 8.

2.3.2 Renal Tubule

The renal tubule can be divided into separate segments differing in structure, function, and position in the kidney: the proximal convoluted tubule, the loop of Henle, the distal convoluted tubule and the connecting tubule. The organization of the renal tubule is shown in Figure 9.

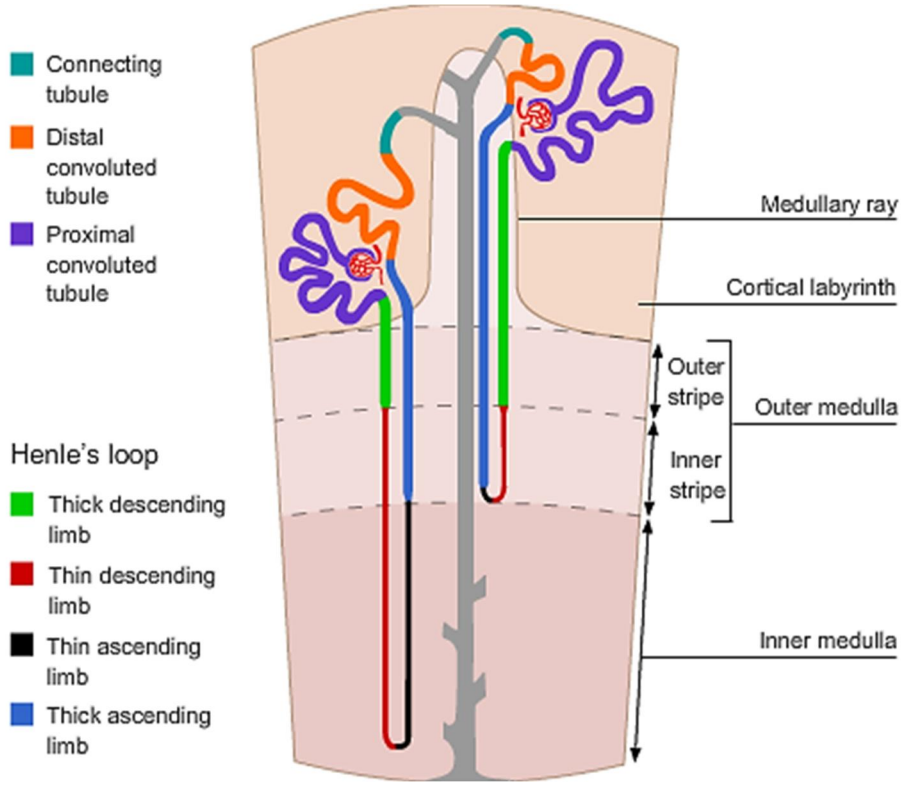

Figure 9: Segmental organization of the renal tubule [1]

The proximal convoluted tubule, which is connected with the Bowman's capsule, is located in the cortical labyrinth where it follows a convoluted path near the renal corpuscle. It then enters the medullary tissue.

The loop of Henle is U shaped segment that connects the proximal convoluted tubules and the distal convoluted tubule. The loop of Henle is formed by four areas: thick descending limb, thin descending limb, thin ascending limb, thick ascending limb. The first part of the descending limb is a continuation from the proximal tubule. The descending limb reaches deep into the medulla, and has low permeability to ions and urea, while water can easily pass through it. After the U turn in the loop and it moves upward to the cortex once again.

The distal convoluted tubule (DCT) is continuous with the thick ascending limb of the loop of Henle. It is located in the cortical labyrinth where it forms tightly compacted loops near the glomerulus.

The connecting tubule is a short straight terminal segment of the renal tubule that connects the DCT to the collecting duct system.

Each renal tubule empties into a collecting system, which is shown in Figure 10. The collecting system begins with the initial collecting tubules, which are located in the cortical labyrinth in continuation with the connecting tubules. [1]

Then they enter a medullary ray, the initial collecting tubules connect to form the cortical collecting duct. Thus, a single collecting duct drains many nephrons [1].

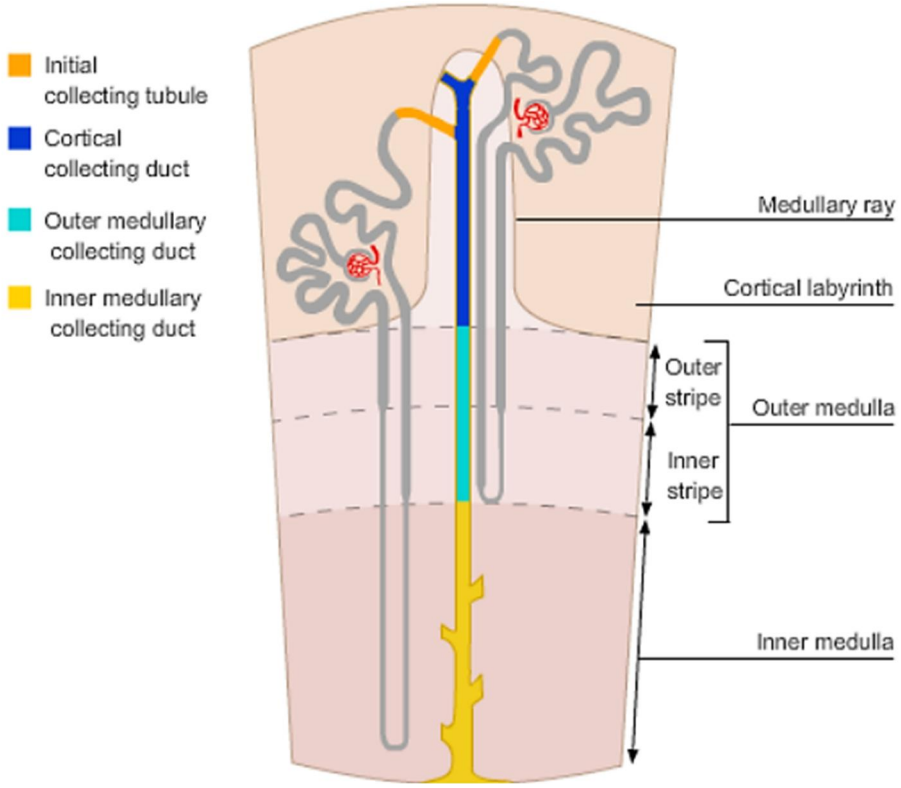

Figure 10: Segmental organization of the collecting system [1]

As it goes down through the medullary ray into the depth of the medullary pyramid, the collecting duct has a higher diameter and is called successively the outer medullary collecting duct and the inner medullary collecting duct (IMCD). In the deeper part of the inner medulla, several IMCD join together to form the papillary ducts, that are larger segments. [1]

2.3.3 The Juxtaglomerular Apparatus

The juxtaglomerular apparatus (JGA) is a system in the nephron that is placed where the ascending limb of Henle's loop meets the glomerular afferent arteriole of the same nephron [1], as shown in Figure 11 (a). JGA consists of all structures that form this site of contact: macula densa, juxtaglomerular cells, and extraglomerular mesangial cells. Figure 11 (b) shows the components of the JGA.

This structure allows the kidney to sense the glomerular filtration rate (GFR) based on the ionic composition of the tubular fluid and to adapt it through the tubuloglomerular feedback (TGF) mechanism and the controlled release of renin.

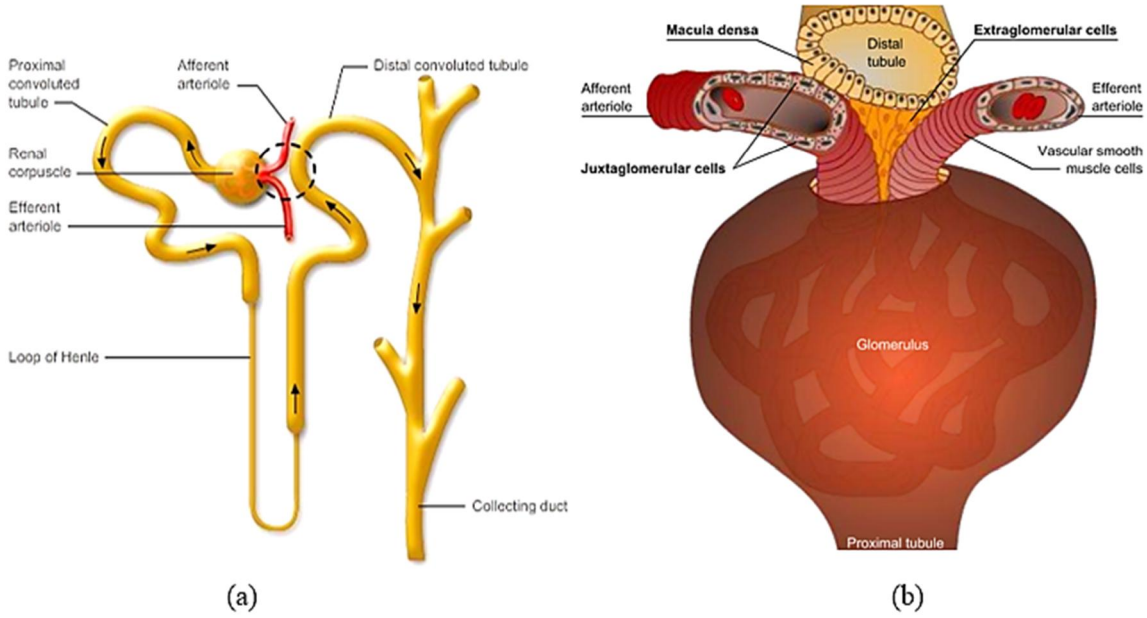

Figure 11: (a) Juxtaglomerular location; (b) Components of the JGA [1]

Macula densa (MD) is a region of approximately 30 specialized tubular cells located in the first part of the distal convoluted tubule. These cells act as sensors. They sense the NaCl concentration in the tubular fluid as an indicator of the GFR and if they measure a change from normal GFR, they send chemical signals that modify the vascular tone of the afferent arteriole, and adjust the level of renin secretion from juxtaglomerular cells. These responses help to maintain a constant GFR even if there are variations in blood pressure during the day. The extraglomerular mesangial cells are placed in the angle formed between the two arteriole, below the macula densa. It seems that the extraglomerular mesangial cells are involved in the secretion of erythropoietin and secretion of renin [1].

3. Renal Physiology

The kidney is responsible for many functions in the human body, but three of these are among the most important: glomerular filtration, tubular reabsorption and tubular secretion.

In order to produce urine, the first necessary step is glomerular filtration: the blood is filtered by the renal corpuscle and in particular, the proteins and large molecules are left out. For this reason the glomerular ultrafiltrate is very similar to plasma, but without proteins.

During tubular reabsorption, water and electrolytes are transported from the tubular filtrate to the peritubular capillaries. This process is fundamental because it is necessary to bring back into the systemic circulation the substances that have been filtered, but that are instead useful for the body.

Finally, tubular secretion involves the transport of waste products, such as ammonia, hydrogen ions and potassium, in order to produce urine [1].

3.1 Glomerular Functions

One of the primary functions of the glomerulus is the glomerular ultrafiltration: it transports fluid and solutes from the glomerular capillaries into Bowman's capsule. Figure 12 shows ultrafiltration that takes place in the renal corpuscle as blood is forced through the glomerular filter.

The filtration barrier of the glomerulus selects substances according to their size and charge, maintaining large and negatively charged macromolecules within the circulation. All molecules below 7,000 daltons are freely filtered, and all those above 70,000 daltons are excluded [2]. Often the composition of the filtrate is an indicator of disease: the presence of large proteins signifies a breakdown in the negative charge of the glomerular capillary membrane, while an abundance of small proteins such as myoglobin and hemoglobin may refer to damaged muscles or erythrocytes respectively.

The kidney filters blood at a rate of 125 ml/min, signifying that the entire blood volume is filtered over 25 times per day. This ultrafiltration is possible thanks to Starling forces, or hydrostatic and oncotic forces, that drive fluid from the glomerular capillaries across the filtration membranes into Bowman’s space. [1]

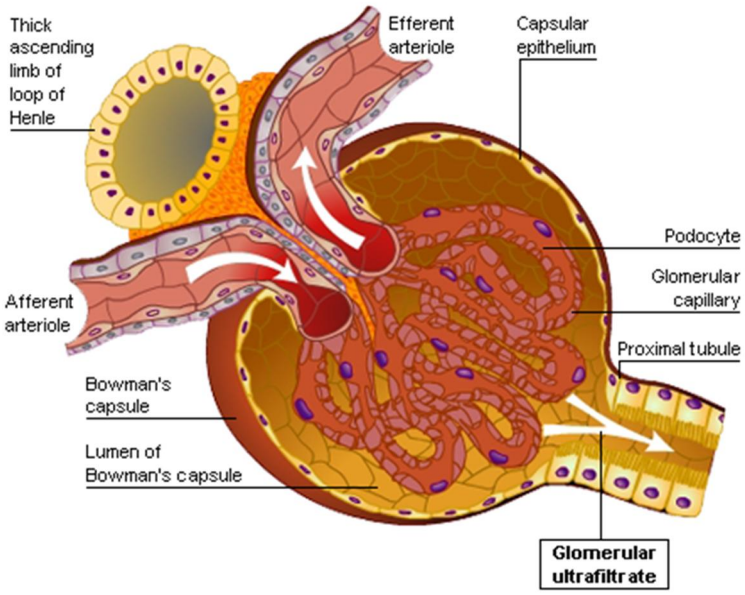

Figure 12: Ultrafiltration in the renal corpuscle. White arrows in the arterioles indicate the direction of blood flow [1]

Figure 13 shows the forces affecting ultrafiltration in the glomerulus. Hydrostatic pressure exists due to fluid forces, while oncotic pressure is a form of osmotic pressure applied by proteins in blood plasma that is needed to pull water into the circulatory system because the proteins in the plasma are too large to pass through the capillary wall. The net filtration pressure is a balance of four pressures, and is higher than the pressure in other capillary beds all over the body [1].

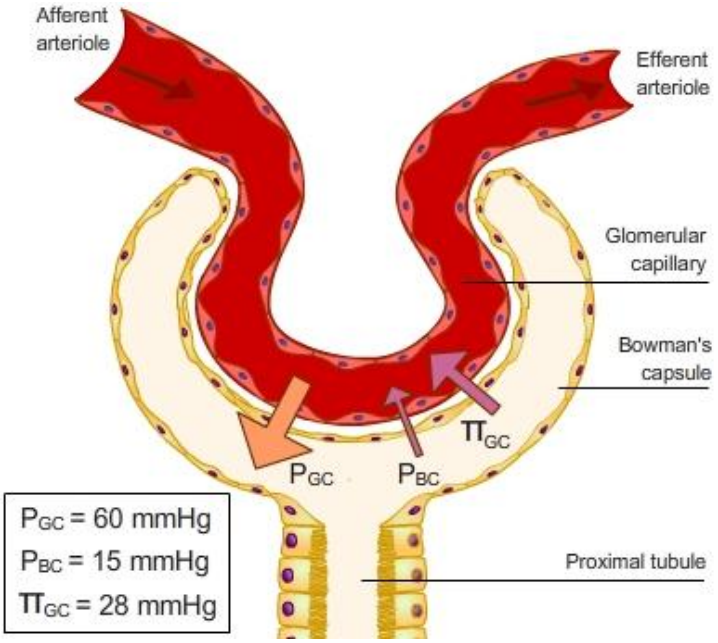

Figure 13: Starling forces that affect the glomerular ultrafiltration and determine the net filtration pressure [1]

Those forces involved in the filtration process are the glomerular capillary hydrostatic pressure (P_{GC}) and the Bowman's capsule oncotic pressure (π_{BC}), while the glomerular capillary oncotic pressure (π_{GC}) and Bowman's capsule hydrostatic pressure (P_{BC}) oppose it.

The direction of the flow is determined by net filtration pressure (P_{UF}), which, according to the Starling equation (3.1), is determined by the difference between the net hydrostatic pressure and the net oncotic pressure.

$$P_{UF} = (P_{GC} - P_{BC}) - (\pi_{GC} - \pi_{BC}) \tag{3.1}$$

The glomerular filtration rate (GFR) is the total amount of filtrate formed by all the renal corpuscles in both kidneys per minute, which is the volume of fluid filtered out of the blood and into Bowman's capsules per unit time. GFR depends on the net ultrafiltration pressure and the ultrafiltration coefficient (K_f) that represents the product of the glomerular capillary hydraulic permeability and the total surface area available for filtration. Equation 3.2 shows this calculation. Typical values in humans are $P_{GC} = 60$ mmHg, $P_{BC} = 15$ mmHg, $\pi_{GC} = 28$ mmHg, and $\pi_{BC} = 0$, leading to a net filtration pressure of 17 mmHg and a GFR of 125ml/min. [1]

$$GFR = K_f * [(P_{GC} - P_{BC}) - (\pi_{GC} - \pi_{BC})] \tag{3.2}$$

An increase in renal arterial pressure temporarily elevates glomerular capillary pressure, thus intensifying GFR. In the same way, a decrease in pressure inhibits GFR. Each of these effects can be compensated by a corresponding change in arteriolar resistance to stabilize GFR and tubular flow. This is the primary consequence of autoregulation, along with stabilizing renal blood flow and protecting the glomeruli from damaging pressure fluctuations [1].

3.2 Tubular Functions

After being collected into the space of Bowman's capsule, the glomerular filtrate moves into the renal tubule, where its composition is modified in order to produce urine. The conversion of glomerular filtrate into urine involves two main processes: tubular reabsorption and tubular secretion.

As a result of tubular reabsorption certain substances of the filtrate are transported back into the systemic circulation: the substances are initially transported from the tubules to the interstitial liquid of the cortex or medulla, and subsequently the substances spread in the blood capillaries. Every day 99% of the filtrate is reabsorbed as it is useful to bring back into the blood all the substances that have been filtered but are essential for the body.

Tubular reabsorption takes place along the different segments of the renal tubule but the proximal tubule is clearly the most active segment in this mechanism [1].

Tubular secretion is the opposite process through which substances move from the peritubular capillary into the renal tubules where they are added to the forming urine.

Tubular secretion serves to eliminate waste products. It is also needed to regulate important body functions. For instance, the tubular secretion of H+ and ammonium helps to regulate the pH of blood and the acid-base balance of the body fluids. Tubular secretion takes place mainly in the distal tubules and collecting ducts. It also occurs in the proximal tubule. [1]

3.3 Oxygen Homeostasis

Living organisms demand for a continuous input of energy to accomplish activities such as active transport of molecules and ions, synthesis of macromolecules, and motion. Energy is produced in the form of adenosine triphosphate (ATP). Oxygen is a fundamental component for cellular energy production because it is the reduction of O2 to water that enables the conversion of ADP into ATP. [1]

Oxygen homeostasis is critical for the correct functioning of the body. In general, it depends on the respiratory and cardiovascular systems. It also depends on the capacity of the blood to carry oxygen, which depends on the amount of haemoglobin in the blood.

In the human body exist primary sensors for monitoring independently the arterial oxygen partial pressure (pO2) and the oxygen concentration (%O2) in the blood, in order to maintain oxygen homeostasis.

When sensing a reduction in arterial pO2, the chemoreceptors send information to start appropriate changes in the activity of the respiratory and cardiovascular systems. When sensing a reduction in arterial O2 concentration, renal fibroblasts release erythropoietin (EPO) that stimulate the production of erythropoiesis.

The respiratory and cardiovascular systems have a fast response; on the contrary, the reaction of kidneys takes time to have effect because it requires synthesis of EPO and its release in the circulation. [1]

3.3.1 Kidney and EPO

The kidneys play an essential role in oxygen homeostasis, regulating the production of erythrocytes. This control is performed thanks to the release of the hematopoietic growth factor erythropoietin, produced by the kidneys as reaction to two main stimuli: reduction in oxygen carrying capacity (anaemic hypoxia) and reduction in arterial oxygen tensions (hypoxic hypoxia) [3].

In the kidney, EPO is synthesized by peritubular interstitial fibroblasts located in the deep cortex at the cortico-medullary junction [4]. These cells are called REP cells (renal erythropoietin-producing cells). REP cells display a stellar shape and are tightly arranged around tubules and vessels [1]. An example is shown in Figure 14.

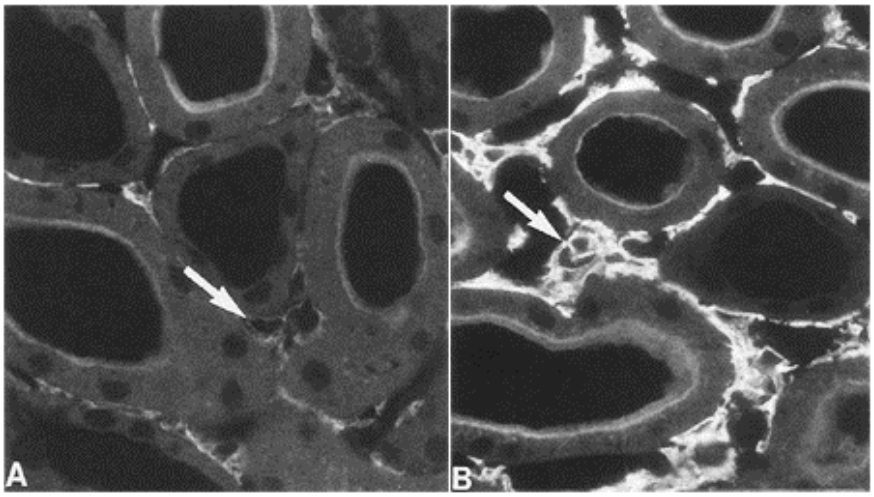

Figure 14: Localization of EPO-producing cells in the rat kidney. Cortical labyrinth of a control rat (A) and of an anaemic rat (B). Anaemia provokes enlargement of the fibroblasts (arrows). [5]

The most productive stimuli for an increase of the EPO concentration in plasma are a decrease in haemoglobin saturation in the arteries, caused by a fall in arterial pO2, or a reduction in the capacity of the blood to carry oxygen (anaemic hypoxia) [3].

Another parameter affecting circulating EPO levels is the affinity to oxygen of haemoglobin. Whereas all of these conditions cause a decrease in the oxygen availability to the tissues, reduced tissue oxygen tension is the principal physiological determinant for expression of the EPO gene in the kidney. [1]

Conditions leading to reduced arterial pO2 values (hypoxia), and consequently to decreased oxygen saturation of erythrocytes haemoglobin, are another important stimulus for increased EPO production.

EPO is the primary, and probably the unique mediator of hypoxic induction of erythropoiesis. It serves to maintain erythropoiesis under steady-state conditions and to accelerate the recovery of red blood cells mass after haemorrhage. Erythropoiesis is a slow-acting process: following a rise in plasma EPO levels it takes 3-4 days before elevation in the number of circulating red blood cells becomes apparent. [1]

4. Modeling Concepts

4.1 Definition of Basic Terms

Phase

The phase is a region of space with a homogeneous chemical composition and physical state. Distinct states of matter as solid, liquid and gas may be defined as different phases.

Component

A component can be a chemical substance or a combination of different chemical substances with comparable characteristics, such as the interstitial fluid or blood. [6] A phase of a given system is constituted of at least one component.

4.2 Definition of Structures and Scales

A biological system can be modelled in two methods: the molecular approach and the continuum approach. The molecular one takes under investigation the motion of single molecules and their interplay under external forces, while the continuum approach assumes that the fluid is continuously distributed over the whole domain. Due to the high number of molecules and particles in fluids, the molecular approach is not suitable for the solution of fluid problems [6]. In this thesis, the fluid phase is described with a continuum approach.

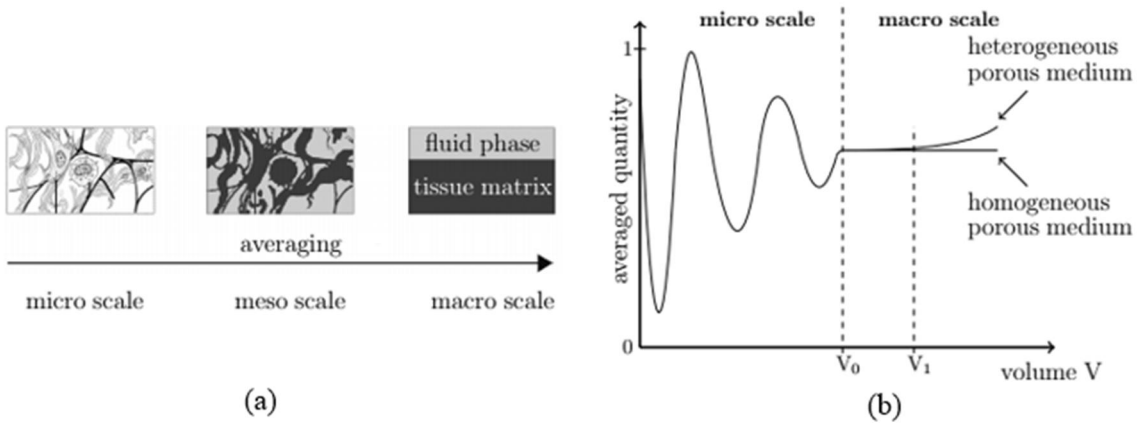

Figure 15: (a) From a biological tissue to a porous medium (b) Definition of the REV [7], [6]

The structure of the biological system can be studied in a discrete or a continuous manner. Figure 15(a) shows the continuum approach for a biological tissue: the left picture in this figure shows the tissue on the micro scale in which the individual components can be clearly distinguished. [6]

The right picture in Figure 15(a) depicts the macro scale: in this case, it is not possible to distinguish the discontinuities that can be recognized in the micro scale. To go from the micro to the macro scale an averaging of the characteristics of the porous medium in the representative elementary volume (REV) is required [6]. It is necessary to choose the representative elementary volume in a way that the averaged property is not influenced by the volume, which is the case between V_0 and V_1, as shown in Figure 15(b).

4.3 Definition of Effective Parameters

The averaging process of the properties of the porous medium creates new effective parameters that are explained in the following:

Porosity

The porosity Φ is defined as the ratio of the volume of the pore in the REV and the REV total volume:

$$\Phi = \frac{\text{volume of the pore space within the REV}}{\text{total volume of the REV}} \tag{4.1}$$

Permeability

The permeability is a measure of the ability of a porous media to allow fluid to pass through it. It characterizes the resistance of a porous matrix to the flowing fluids. The intrinsic permeability K is defined as follows:

$$\mathrm{K} = -\frac{Q\mu L}{\Delta p A} \tag{4.2}$$

It is derived from Darcy's law. Here, Q represents the flow rate of a fluid, μ is the dynamic viscosity, A is the area through which flows the fluid, L is the length, and everything is driven by the pressure difference Δp.

4.4 Definition of Fluid Properties

Density

The density is a physical quantity that characterizes a fluid and it depends on the composition of the phase. It is possible to identify the mass density and the molar density of a phase. The mass density is the ratio of mass *m* and volume *V*:

$$\rho_{mass} = \frac{m}{V} \tag{4.3}$$

The molar density is defined as:

$$\rho_{mol} = \frac{n}{V} \tag{4.4}$$

Where *n* is the number of moles.

Viscosity

The viscosity of a fluid is a measure of its resistance to deformation caused by shear or tensile stress. The dynamic viscosity μ is the ratio of the shear stress τ and the velocity gradient $\frac{dv}{dy}$. Hence, the shear stress τ is proportional to the velocity gradient and the dynamic viscosity μ:

$$\tau = \mu \frac{dv}{dy} \tag{4.5}$$

The kinematic viscosity instead is the ratio between the dynamic viscosity μ and the density of the fluid ρ:

$$\nu = \frac{\mu}{\rho} \tag{4.6}$$

5. Numerical Model and Implementation

5.1 Vascular tree Representation

In order to study flow and oxygen transport in the kidney, an anatomically accurate model of the renal vasculature is required. Nordsletten et al. [8] have developed an automatic segmentation technique to two renal micro-computer tomography (CT) images acquired from a rat. Microcomputed tomography (micro-CT) offers the ability to produce high-resolution detailed images and to obtain information on the vascular structures. In order to organize and tabulate vascular data, Nordsletten et al. applied the Strahler Order [9], an algorithm originally developed for stream ordering, and found to be highly applicable to vascular branching. An example of Strahler ordering is shown in Figure 16. According to the Strahler ordering, the terminal arterioles are labelled with order 0. Considering the upstream path of the vessel, if two order 0 vessel merge together creating a bifurcation, the order of the parent vessel is set to 1, while if an order 0 vessel merges with a vessel of different order, the parent assumes the value of the highest order vessel [9].

This method is particularly suitable for the kidney due to the lack of connections between vessels [8].

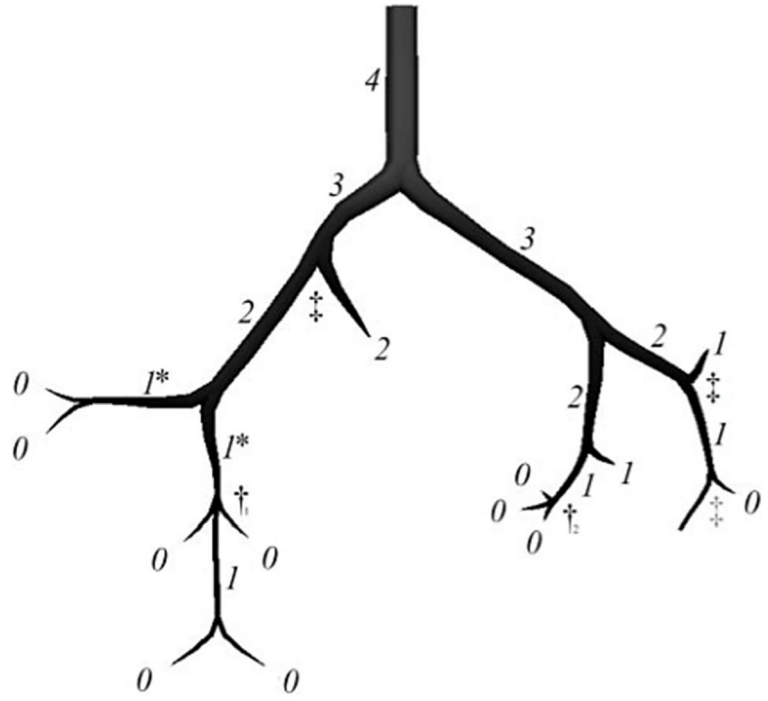

Figure 16: Example of vascular tree using Strahler Ordering, reprinted from [8]

Nordsletten et al. initially have used a 20-µm voxel resolution image to segment the arterial and venous trees for the rat vasculature, distinguishing vessels down to 30 µm in radius. It was followed by the segmentation of a higher resolution 4-µm voxel image of a renal vasculature subtree, with vessel radial values lower than 10 µm.

An iterative scheme was developed by Nordsletten to integrate the two parts of information and map the renal vascular tree. For further information regarding the reconstruction process, the reader is referred to [8].

5.2 Data Processing

The data provided by Nordsletten was processed using the graphical user interface CMGUI, an advanced 3D visualisation software package with modelling capabilities [10]. The data from Nordsletten [8] was created and processed using this software itself which motivated its use for our studies. Nordsletten made available the vascular network in *exelem* and *exnode* file format - data format required by the CMGUI - for both the arteries and the veins. Detailed process to analyze a data in such a format using CMGUI is detailed below.

From the Command Window, one can easily read the *element* and *node* file from the standard menu, or by typing in the Command Line the following commands:

```
gfx read nodes
```

```
gfx read elements
```

This process needs to be executed for both the arteries and the veins files. Once the nodes and elements have been read it is possible to visualize a surface from the Scene Editor. The Scene Editor is used to control how visualizations appear in the Graphics Window. From this window, it is possible to toggle visibility for any part of the region tree, to toggle visibility of any individual graphics setting for a region, and finally add, remove, and edit graphics.

For the sake of making clear what kind of format is stored, the following shows part of the *exelem* and *exnode* files respectively.

Exelem

```
Group name: Veins
Shape. Dimension=1
#Scale factor sets=1
c.Hermite, #Scale factors= 4
#Nodes= 2
#Fields=2
```

```
1) coordinates, coordinate, rectangular  cartesian, #Components=3
  x.  c.Hermite, no modify, standard node based.
   #Nodes= 2
     1. #Values=2
        Value indices:     1  2
        Scale factor indices:      1  2

     2. #Values=2
        Value indices:     1  2
        Scale factor indices:      3  4

  y.  c.Hermite, no modify, standard node based.
   #Nodes= 2
     1. #Values=2
        Value indices:     1  2
        Scale factor indices:      1  2
     2. #Values=2
        Value indices:     1  2
        Scale factor indices:      3  4
  z.  c.Hermite, no modify, standard node based.
   #Nodes= 2
     1. #Values=2
        Value indices:     1  2
        Scale factor indices:      1  2
     2. #Values=2
        Value indices:     1  2
        Scale factor indices:      3  4

2) general,field,rectangular cartesian,#Components= 2
  1. c.Hermite, no modify, standard node based.
   #Nodes= 2
     1. #Values=2
        Value indices:     1  2
        Scale factor indices:      1  2
     2. #Values=2
        Value indices:     1  2
        Scale factor indices:      3  4

  2. c.Hermite, no modify, standard node based.
   #Nodes= 2
     1. #Values=2
        Value indices:     1  2
        Scale factor indices:      1  2
     2. #Values=2
        Value indices:     1  2
        Scale factor indices:      3  4

  Element: 1  0  0
     Nodes:
        1      2
     Scale factors:
        1.0E+0  1.0E+0  1.0E+0  1.0E+0
```

Exnode

```
Group name: Veins
#Fields=2
1) coordinates, coordinate, rectangular cartesian, #Components=3
x.  Value index=1, #Derivatives=1 (d/ds1)
y.  Value index=3, #Derivatives=1 (d/ds1)
z.  Value index=5, #Derivatives=1 (d/ds1)

2) general, field, rectangular cartesian, #Components= 2
1.  Value index= 7, #Derivatives=1 (d/ds1)
2.  Value index= 9, #Derivatives=1 (d/ds1)

Node: 1
6886.9734840000001    0.00000000000E+0
10968.180246000002    0.00000000000E+0
15282.825120000001    0.00000000000E+0
54.114976800000001    0.00000000000E+0
4.                    0.00000000000E+0

Node: 2
6919.6273199999996    0.00000000000E+0
11004.959034          0.00000000000E+0
15304.029569999999    0.00000000000E+0
51.572171699999998    0.00000000000E+0
4.                    0.00000000000E+0

Node: 3
6949.4722019999999    0.00000000000E+0
11022.408719999999    0.00000000000E+0
15318.837090000001    0.00000000000E+0
49.973569740000002    0.00000000000E+0
4.                    0.00000000000E+0
```

From the Scene Editor it is possible to create the visualization of the surface adding cylinders in the Graphics List, and by defining other parameters like the subgroup fields (Veins or Artery in this case), the radius value, the tessellation (used to set the level of detail of an object), the circle discretization, the material and so on. Figure 17 shows an example of the parameters that can be set in the Scene Editor of the CMGUI.

As an alternative, it is possible to write in the Command Line the following lines of code that does exactly what was explained before.

```
gfx modify g_element Veins cylinders radius general.1 material white

gfx modify g_element MaArtery cylinders radius general.1 material red

gfx modify g_element MiArtery cylinders radius general.1 material red
```

The command `radius general.1` means that value of the radius considered to reconstruct the surface of the vessels is the one detected by Nordsletten et al., which is stored in the nodes file. The values of the radius are shown in Table 1 and Table 2 for the arterial tree and venous tree respectively.

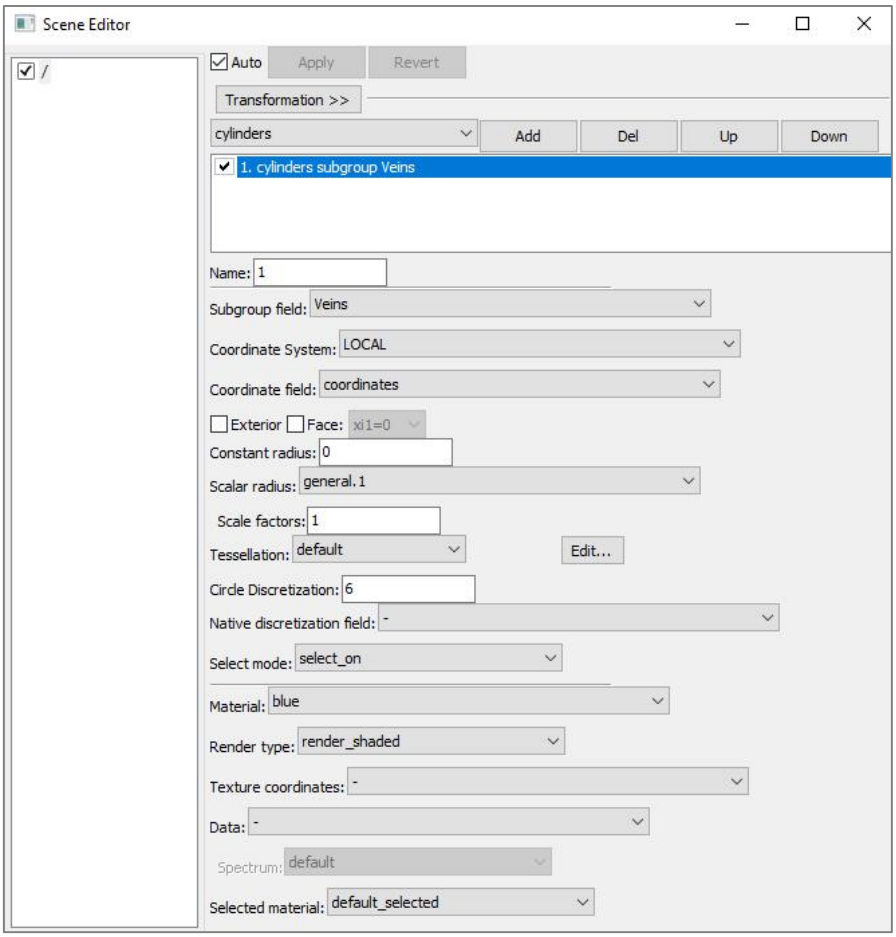

Figure 17: Example of the Scene Editor of the CMGUI

Order	Radius μm
0	10.08 ± 0.14
1	13.90 ± 3.80
2	20.06 ± 6.90
3	29.87 ± 0.35
4	39.29 ± 1.08
5	44.23 ± 9.81
6	53.87 ± 12.51
7	86.15 ± 24.06
8	139.83 ± 20.11
9	191.42 ± 17.79
10	216.10 ± 4.74

Table 1: Radius in µm of the renal arterial tree [8]

Order	Radius μm
0	10.79 ± 2.41
1	14.72 ± 4.05
2	26.16 ± 1.57
3	40.13 ± 8.51
4	50.30 ± 12.12
5	69.22 ± 21.18
6	114.07 ± 29.59
7	177.04 ± 39.04
8	285.63 ± 52.86
9	428.05 ± 80.95
10	603.77 ± 94.52

Table 2: Radius in µm of the renal venous tree [8]

After that the parameters of interest have been set in the Scene Editor, to obtain a more smoothed surface using the "gfx smooth" command, which uses an averaging method for calculating smooth derivatives:

```
gfx smooth field coordinates
```

The effect of the "gfx smooth" command is shown in Figure 18. It is possible to notice that before applying the "gfx smooth" command (Figure 18 a) the surface of the vessels presents gaps where the cylinders should merge. After the smoothing most of the gaps are removed (Figure 18 b), even if at the vessels bifurcations some artefacts are still present.

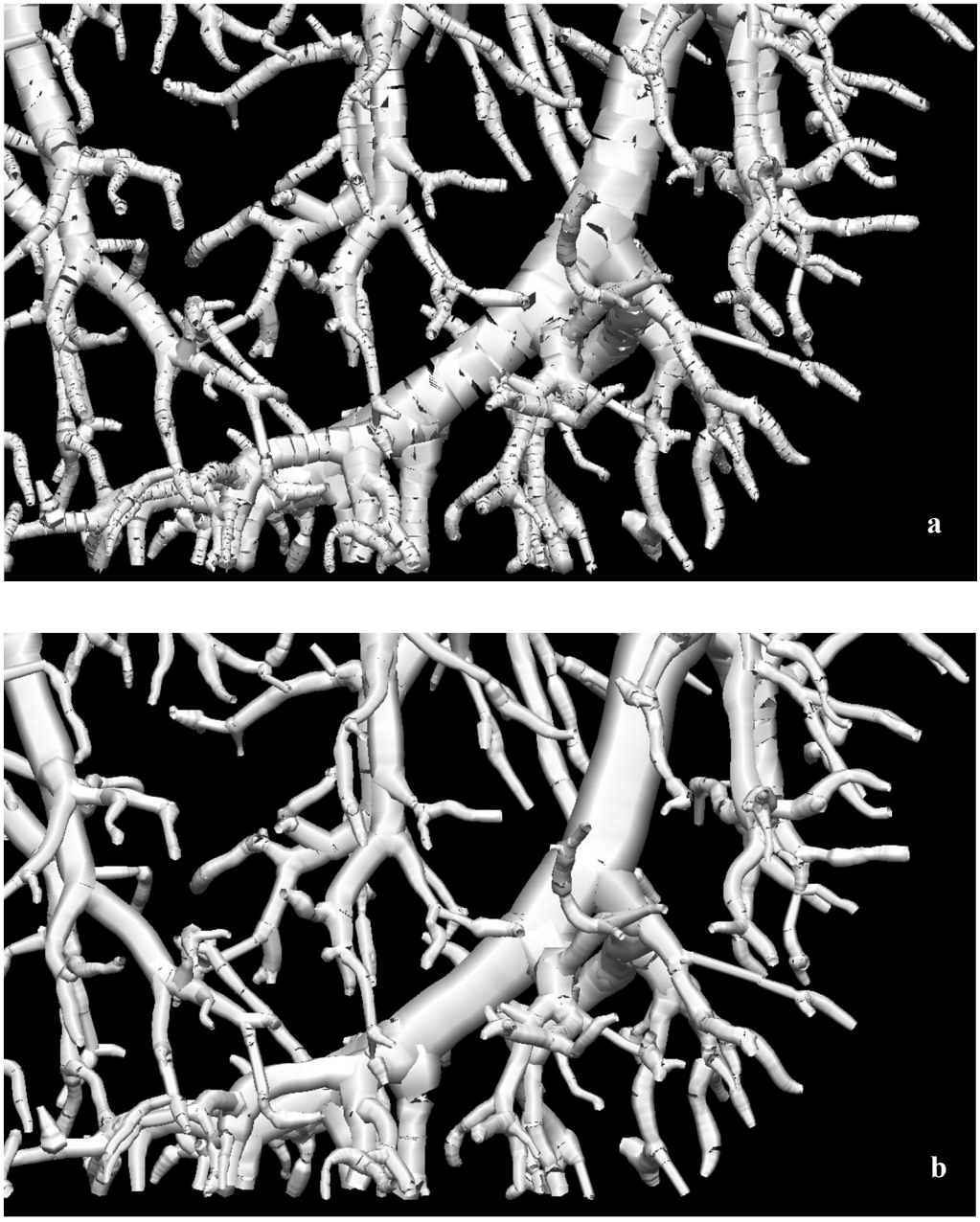

Figure 18: Effect of the smooth on CMGUI. (a) Venous tree before applying the smooth command; (b) Venous tree after the smooth

In order to visualize the obtained geometry, a Graphics Window should be created. The Graphics Window is where all visualizations set up in the Scene Editor are displayed. It also has tools which allow some interactive manipulation of the data being visualized. Furthermore, the Graphics Window provides the ability to save the viewing area as a raster graphic, such as a png or jpg file.

Figure 19 shows the reconstructed model of renal arterial and venous trees, where the arteries are represented in red and the veins in white.

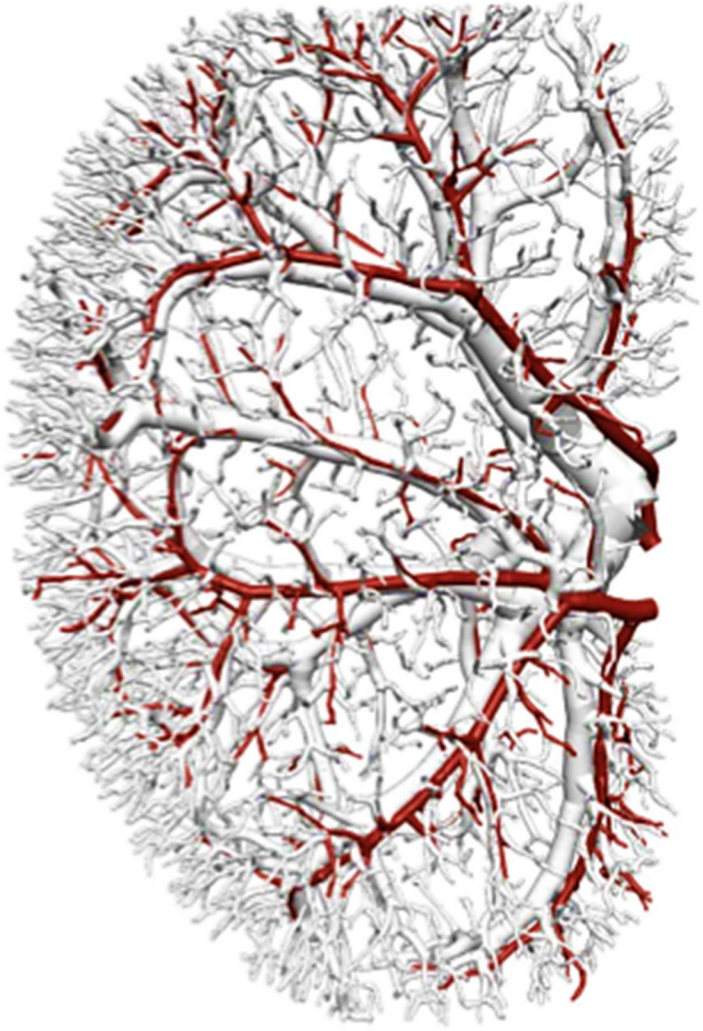

Figure 19: Reconstructed model of renal arterial and venous trees. The arteries are represented in red, the veins in white.

The obtained surface has been saved in a STL (STereo Litography interface format) file in order to have a format readable by Paraview, a multi-platform data analysis and visualization application. The following command has been executed in the Command Line interface:

```
gfx export stl file kidney.stl
```

The stl file obtained from CMGUI was then visualized using Paraview to obtain a deeper insight in the geometry whether it was suitable to carry out simulations or not. Artefacts, especially at the bifurcations were noticed, which are highlighed inside the red circles in Figure 20.

The presence of these artefacts made the obtained 3D surface mesh unsuitable for simulation studies, which motivated a fall-back into 1D studies (see results section 6.2).

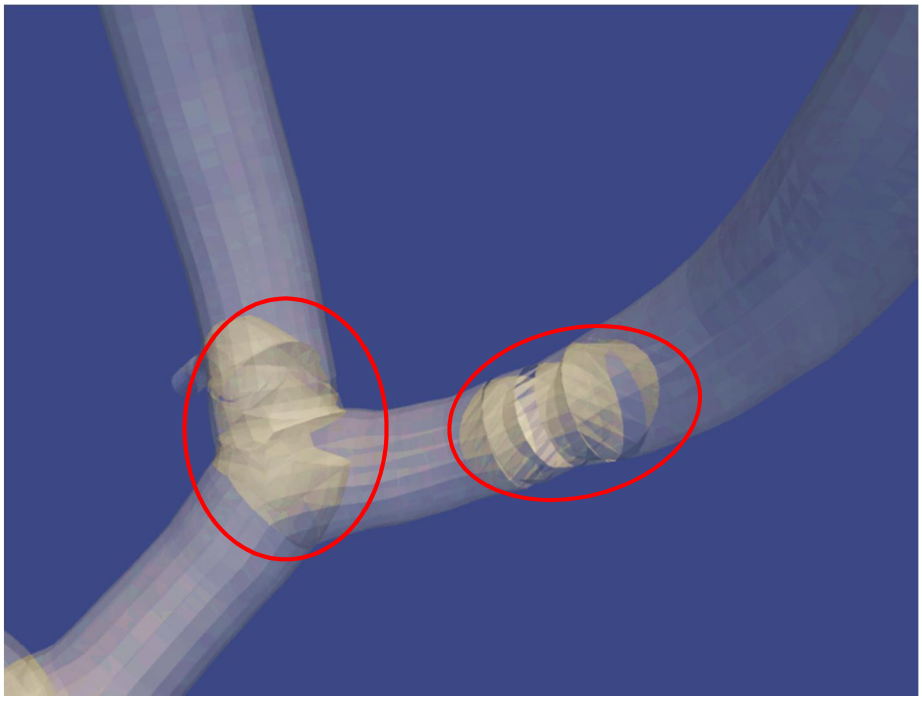

Figure 20: Example of artefacts inside the vessels

This might be related to the quality of the mesh, i.e. there are neighbouring elements that differs in size and, furthermore, the bifurcations have a single derivative, meaning that where two vessels join into one, all three vessels must be collinear. In order to fix this problem, manual intervention was triedto remove the artefacts using Blender, a 3D computer graphics software. This approach was however not successful, thus for the further studies the 1D network has been adopted.

In parallel, investigations revealed that to use this model for 3D simulations, a surface modeling approach will need to be adopted. For this, methods within the Vascular Modeling ToolKit (VMTK) were explored. The centerlines, already provided by Nordsletten [8] could be read by VMTK and the surfacemodeler within VMTK could then produce a 3D surface mesh of high quality - free from the aforementioned artefacts.

Towards the end of the thesis, we found that to process a small section of the kidney using VMTK required about 70 hours of execution time on a workstation. Thus, this approach was considered prohibitive to achieve a full 3D surface mesh of the data. It is however recommended that a parallelization approach which can be implemented within VMTK can help to obtain 3D surface meshes. Due to time restrictions, this was not explored within the context of this thesis.

5.3 Literature Review of Renal Oxygenation Model

The dynamics of renal oxygenation is poorly understood. It is known that "hypoxia may occur in the renal cortex or in the medulla, causing possible tissue damage and leading to both chronic and acute kidney diseases" [11]. There are a few studies on the renal oxygenation modeling based on the data provided by Nordsletten. For example, Gardiner et al. [12] suggest a mathematical model of oxygen transport in the renal cortex to understand "how arterial-to-venous (AV) oxygen shunting influences kidney oxygenation". Their model consists of a multiscale hierarchy of 11 countercurrent compartment connected in series, representing the various branch levels of the cortical vasculature. Gardiner et al. model predicts that "the quantity of oxygen shunted from arteries to veins increases with increasing oxygen consumption and with increasing arterial blood P_{O2}".

Olgac and Kurtcuoglu [13] developed a computational model that takes into account transport process in arteries, veins, cortical tissue and capillaries. Their model is based on an extension of the single dimensional approach used by Gardiner et al. to a segment-wise three-dimensional description of oxygen transport. Olgac and Kurtcuoglu suggest that "cortical tissue oxygenation is determined mainly by the interaction between oxygen perfusion and consumption in the tissue, but not by the arterial-to-vein (AV) shunting in the preglomerular vasculature". They further show that the "preglomerular vasculature is the main source of oxygen when cortical consumption is high or renal artery blood is highly oxygenated. On the contrary, when oxygen demand in the tissue is decreased, or under hypoxemic conditions, oxygen is supplied mainly by capillaries".

5.4 Mathematical Model

Mathematical models have been applied in order to describe the blood flow in the renal vessels and in the surrounding tissue. The vascular tree of the kidney is represented by a 1D network, which is embedded in a 3D domain representing the capillary beds.

In general, one-phase flow can be described by balance equations for mass and momentum. To briefly derive a mass balance, we consider a change of mass within the system, which generate a storage term indicated by M. Mass may be transported over the boundary that yields a flux term A. Sources or sinks within the control volume are denoted by Q. In the need of mass conservation, the mass balance can be formulated for the single-phase:

$$M + A = Q \tag{5.1}$$

Fluid phases within the control volume Ω comprise the mass $\int_\Omega S\rho \, d\Omega$. However, the saturation S in a single-phase is always 1, and the phase occupies only the available pore space Φ, so the storage term M can be formulated as follows:

$$M = \frac{\partial}{\partial t}\int_{\Omega} \Phi\rho \, d\Omega \tag{5.2}$$

We get the flux term A over $\boldsymbol{\Omega}$ by applying the Gauss integral theorem obtaining the flows over the boundary:

$$A = \int_{\Omega} \nabla \cdot (\Phi\rho\mathbf{v}) \, d\Omega \tag{5.3}$$

Production or removal due to external sources or sinks is given as follows:

$$Q = \int_{\Omega} \mathrm{q} \, d\Omega \tag{5.4}$$

Inserting the terms (5.2), (5.3) and (5.4) into equation (5.1), we obtain:

$$\frac{\partial}{\partial t}\int_{\Omega} \Phi\rho \, d\Omega \; + \int_{\Omega} \nabla \cdot (\Phi\rho\mathbf{v}) d\Omega = \; \int_{\Omega} q \, d\Omega \tag{5.5}$$

Equation (5.5) can also be written in differential form as

$$\frac{\partial(\Phi\rho)}{\partial t} \; + \; \nabla \cdot (\Phi\rho\mathbf{v}) = \; q \tag{5.6}$$

Generally, the term **v** has to be expressed by a solution of the Navier-Stokes equations, which describes the flow on the pore scale. However, within the concept of a REV, Darcy's law may be used as a momentum equation:

$$\mathbf{v} = \; -\frac{K}{\mu}(\nabla p - \; \rho g) \tag{5.7}$$

Where, K is the permeability, μ is the viscosity and p is the pressure. Replacing **v** with equation (5.7), equation (5.6) results in:

$$\frac{\partial(\Phi\rho)}{\partial t} \; + \; \nabla \cdot \left[-\rho\frac{K}{\mu}(\nabla p - \; \rho g)\right] = \; q \tag{5.8}$$

Porosity is kept constant and may be thus excluded from the partial expression of the storage term.

$$\Phi\frac{\partial\rho}{\partial t} \; + \; \nabla \cdot \left[-\rho\frac{K}{\mu}(\nabla p - \; \rho g)\right] = \; q \tag{5.9}$$

5.5 Implementation in DumuX

DumuX is an open source software for the simulation of computational fluid dynamics processes in porous media using continuum mechanical approaches. It is possible to use DumuX if also DUNE (Distributed and Unified Numerics Environment) is installed, because DumuX works on the top of it [14].

DumuX involves different standard models of varying complexity, differing from stationary isothermal single-phase single-component flow to transient non-isothermal multi-phase compositional flow. All models make use of efficient nonlinear solvers in solid combination with a time step management. DumuX focuses on different applications, i.e. fuel cells, groundwater remediation, evaporation from partially saturated soils, and even in the medical field with drug delivery in the human body.

DumuX is structured with modularized objects, facilitating the user to choose the proper parts according to the problem to solve [15]. These shelves of modularized objects includes:

- model concepts
- numerical schemes
- control strategies for the simulation
- multitude of substances, material laws
- small and large-scale examples and applications

Figure 21 shows DumuX modular setup.

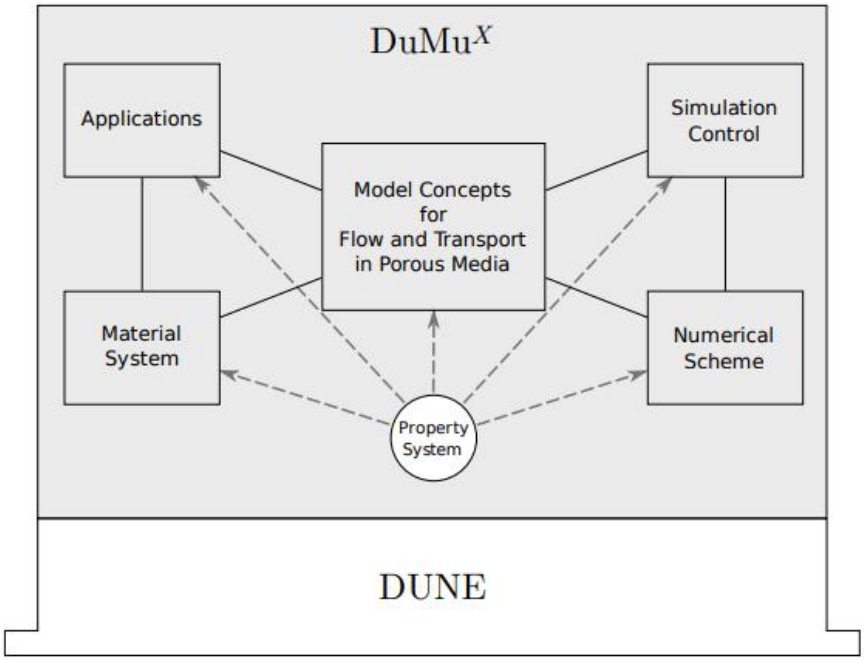

Figure 21: Modular design of DumuX [15]

5.5.1 DumuX Structure

DuMux has the following folder structure [16]:

• **bin**: contains binaries, for example used for the automatic testing.

• **cmake**: the configuration options to build DumuX.

• **dumux**: the main folder that contains the source files.

- `common`: it contains general methods shared by all models.
- `freeflow`: single-phase free-flow models.
- `geomechanics`: models for solving rock mechanics and flow.
- `implicit`: contains the general methods shared by all implicit models, and the specialized methods for the two discretization types box and cellcentered.
- `io`: additional in-/output possibilities
- `linear`: contains linear solver backends.
- `material`: contains all material parameters and constitutive equations.
- `multidomain`: coupling conditions for connecting different model in different subdomains.
- `nonlinear`: Newton's method.
- `parallel`: helper files for parallel simulations.
- `porousmediumflow`: contains all models for porous media setups.
- `sequential`: contains the general methods shared by all sequential models.

• **test**: tests for every numerical model. The structure is the same of the dumux folder. Each test program consist of source `*.cc`, the problem definition `*problem.hh`, the definition of the spatially dependent parameters `*spatialparameters.hh` and an input file `*.input`.

The problem definition file `*problem.hh` is the most important. In this file are set all the basic concepts necessary to solve the problem, i.e. the definition of the boundary conditions. In DumuX, many properties of the porous medium can depend on the spatial location: the intrinsic permeability, the parameters of the capillary pressure and the porosity. Such parameters are specified in the spatial parameters class `*spatialparameters.hh` [16]. Other parameters necessary to solve the problem are stored in the input file. These include i.e. the type of grid, the refinement, parameters useful for the considered component like the viscosity of the fluid, and even settings on the time discretization. Finally, the main file `*.cc` has to be compiled and executed in order to solve the problem and to obtain the outputs that can be read with ParaView to see the graphics results.

DUNE uses the concept of co-dimensional entities: an entity of co-dimension 0 constitutes a cell; the faces between cells are co-dimension 1 entities, and so on until co-dimension *n,* which are the cell's vertices. DUNE also is build in modules, and in particular, DumuX requires dune-common, dune-grid, dune-istl, and on dune-localfunctions. For further information, the reader is referred to [16].

In the following three paragraphs the Newton's method for solving the differential equations on DumuX, the time discretization method and the space discretization method are described.

5.6 Newton's Method

DumuX generates the linear system automatically and implements the differential equations in the residual form. The Newton's method is adopt to solve the differential equations. All terms of the equation are on the left side and are summed up. The terms contain values for the primary variables, which are part of the solution vector $\boldsymbol{u}$. For example:

$$\underbrace{\phi\frac{\partial\rho}{\partial t}-\nabla\cdot\left(\rho\frac{K}{\mu}(\nabla p-\rho g)\right)-\ q=0}_{=:r(u)} \tag{5.10}$$

Is not possible to know the solution $\boldsymbol{u}$, so the iterative Newton's method is needed in order to obtain a good measure of $\boldsymbol{u}$. It start with and initial supposition $\boldsymbol{u^0}$ and compute its residual $\boldsymbol{r(u^0)}$. To minimize the error, it computes the derivative of the residual with respect to the solution. The equation 5.11 represents the Jacobian matrix.

$$\frac{d}{d\boldsymbol{u}}\boldsymbol{r}(\boldsymbol{u}^i) = J_{\boldsymbol{r}(\boldsymbol{u}^i)} = \left(\frac{d}{d\boldsymbol{u}_m^{\boldsymbol{i}}}\boldsymbol{r}(\boldsymbol{u}^i)_n\right)_{m,n} \tag{5.11}$$

With i denoting the Newton iteration step. Each column is the residual derived with respect to the mth entry of $\boldsymbol{u}^{\boldsymbol{i}}$. The Jacobian indicates the direction where the residual increases [15]. By solving the linear system

$$J_{\boldsymbol{r}(\boldsymbol{u}^i)} \cdot x^i = \boldsymbol{r}(\boldsymbol{u}^i) \tag{5.12}$$

it is possible to compute the direction of maximum growth x^i, which is then subtracted from the current solution, in order to get a new and better solution

$$u^{i+1} = u^i - x^i \tag{5.13}$$

The calculation of the Jacobian $J_r(u^i)$ and the direction of maximum growth x^i will be repeated until the approximated solution becomes enough suitable.

5.7 Time Discretization: Euler Method

For the time discretization, the implicit Euler scheme is used. An implicit method evaluates the equations on the new time level (see Figure 22). In the implicit Euler scheme, time-step sizes are not generally restricted by stability. For the transport equation, the time discretization with the implicit Euler method leads to:

$$\frac{\partial u_p}{\partial t} \approx \frac{u_p^{t+\Delta t} - u_p^t}{\Delta t} = f(u_p)^{t+\Delta t} \tag{5.14}$$

The expression $f(u_p)^{t+\Delta t}$ represents the equation that is evaluated at the new time level $t + \Delta t$.

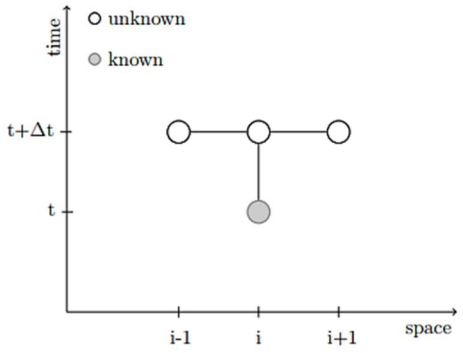

Figure 22: Implicit time discretization [7]

5.8 Spatial Discretization Scheme: Cell Centered Finite Volume Method

The cell centered finite volume method adopts the elements of the grid as control volumes [16]. For each control volume, all discrete values are defined at the element/control volume center as shown in Figure 23.

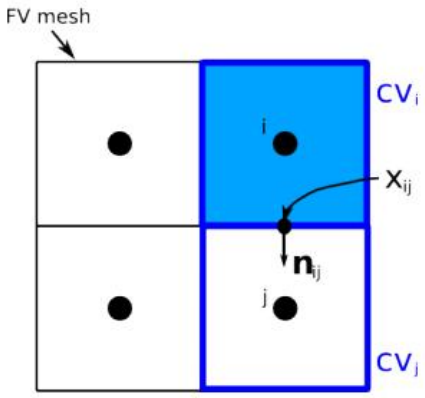

Figure 23: Discretization of the cell centered finite volume method [16]

The mass fluxes are computed at the integration points x_{ij}, which are placed in the center of the control volume faces.

This represents a two-point flux approximation (TPFA) because the flux is calculated just with the information that comes from the element and control volumes centers i and j. Neumann boundary conditions are set at the boundary control volume faces while Dirichlet boundary conditions are imposed at the boundary control volumes.

6. Results

Computations were performed on several micro and macro vasculature networks. Results in terms of pressure drop from inlet to outlet were analyzed and the diffusion from vascular walls into the tissue was observed qualitatively.

The model basically solves Incompressible Stokes equations in 1D to compute pressure profiles, velocity traces and diffusion in the tissue.

6.1 Preliminary Results on Microvascular Networks

In the following paragraph, some preliminary results on microvascular networks are shown. The study conducted on DumuX includes simulations on tumor vasculature, cardiac vasculature and brain vasculature, networks provided by Secomb et al [17]. Each 1D vascular network is embedded in a 3D domain.

6.1.1 Tumor

The tumor network geometry was derived from confocal microscopic observations of mammary carcinoma (R3230AC) implanted in a rat dorsal skin flap preparation [17]. The vascular tree is embedded in a box of 550 x 520 x 230 microns.

Table 3 shows the spatial parameters set for this test case. In particular, the permeability is a relative factor that defines the permeability of vessel walls and the diffusion into surrounding 3D grid.

Spatial Parameters	
Tissue Permeability [m^2]	1.0
Vessel Permeability [m^2]	1.0

Table 3: Spatial parameters for the tumor model

Table 4 shows the boundary conditions: pressure input here means the pressure applied as BC at inlet of the 1D network. Delta pressure signifies the difference of pressure between inlet and outlet thus driving the flow through a pressure gradient.

Boundary Conditions (1D)	
Pressure Input [Pa]	2.0
Delta Pressure [Pa]	1.0

Table 4: Boundary conditions on pressure for the tumor 1D microvascular network

Figure 24 shows the pressure profile in the 1D tumor network.

In particular, it shows the pressure drop from inlet to outlet: from 3.1 Pa in the inlet to 1.2 Pa in the outlet.

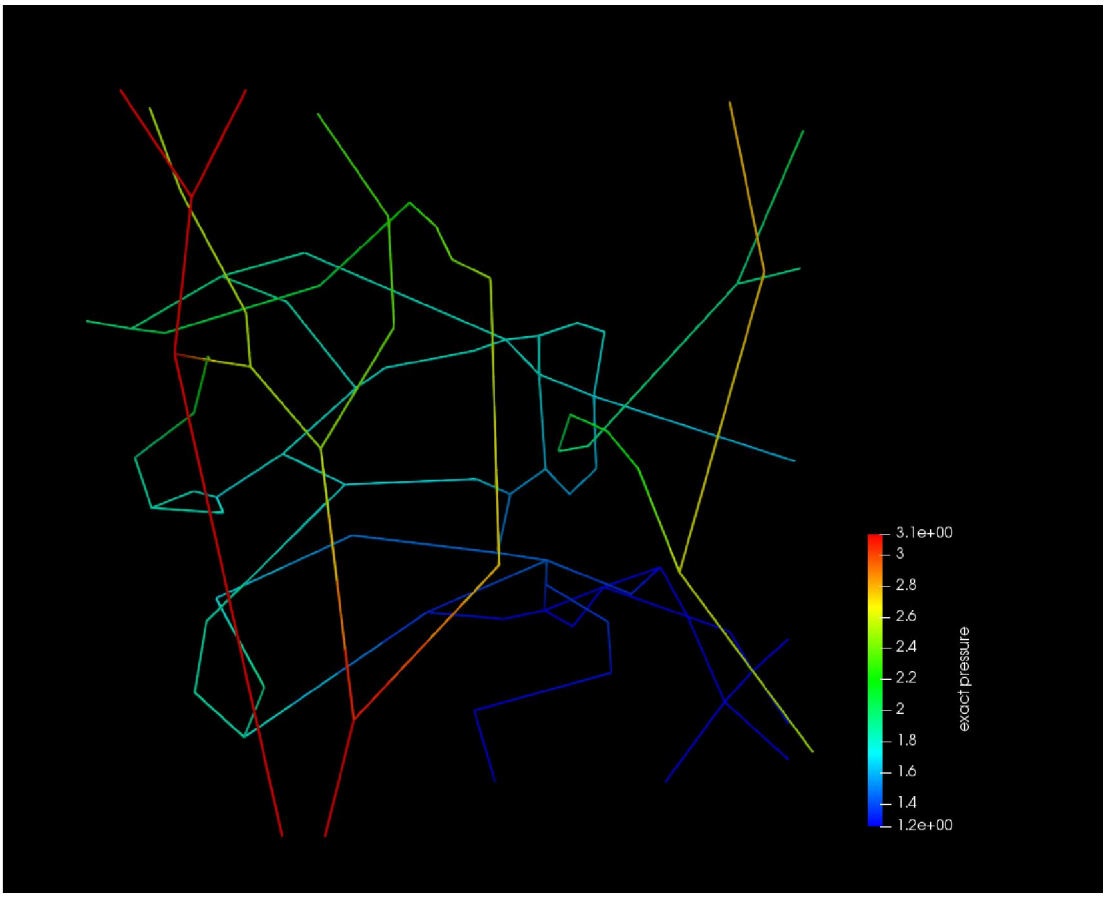

Figure 24: Pressure profile [Pa] in the 1D tumor network

6.1.2 Cardiac

This model represents a coronary sub-network, embedded in a 420 x 241 x 250 microns box. Table 5 and Table 6 show the spatial parameters and the boundary conditions set for this test case respectively.

Spatial Parameters	
Tissue Permeability [m^2]	1.0
Vessel Permeability [m^2]	1.0

Table 5: Spatial parameters for the cardiac model

Boundary Conditions (1D)	
Pressure Input [Pa]	2.0
Delta Pressure [Pa]	1.0

Table 6: Boundary conditions on pressure for the cardiac 1D microvascular network

Figure 25 shows the pressure profile in the 1D cardiac network. In particular, it shows that there is a pressure drop from inlet to outlet of 2.5 Pa.

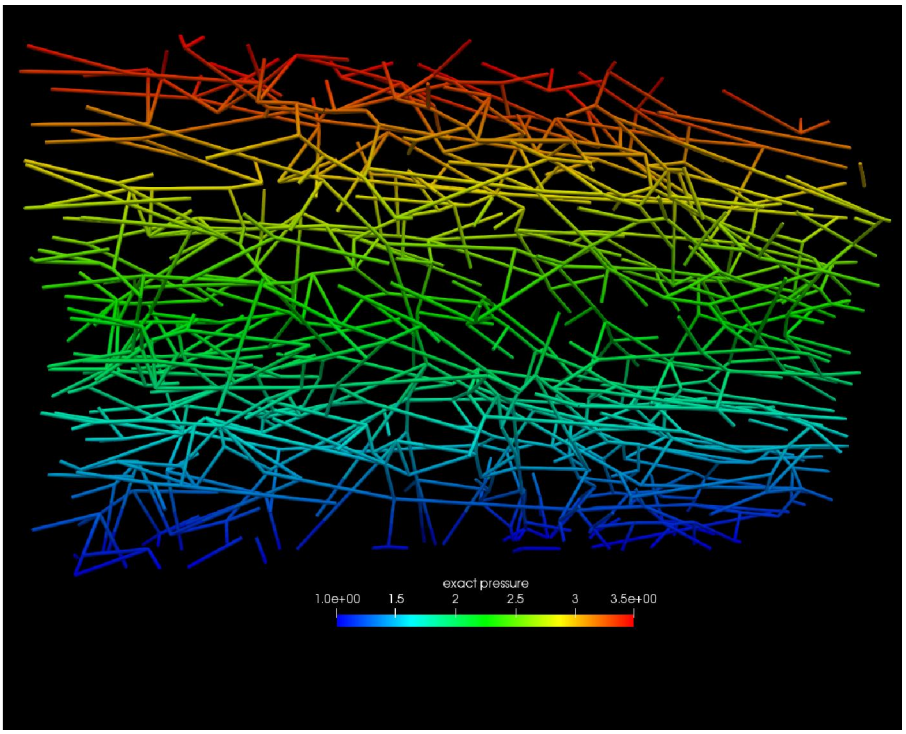

Figure 25: Pressure profile [Pa] in the 1D cardiac network

6.1.3 Brain

This microvascular network represents a rat brain vasculature. The brain network geometry has been obtained by analyzing paired scanning electron micrographs of vascular corrosion casts in the rat superficial cortex [17]. Table 7 and Table 8 show the spatial parameters and the boundary conditions set for this test case respectively.

Spatial Parameters	
Tissue Permeability [m^2]	1.0
Vessel Permeability [m^2]	1.0

Table 7: Spatial parameters for the brain model

Boundary Conditions (1D)	
Pressure Input [Pa]	2.0
Delta Pressure [Pa]	1.0

Table 8: Boundary conditions on pressure for the brain1D microvascular network

Figure 26 shows the pressure profile in the 1D brain network. In particular, it shows the pressure drop from inlet to outlet. From 2.4 Pa in the inlet, the pressure decrease until 1.1 Pa in the outlet.

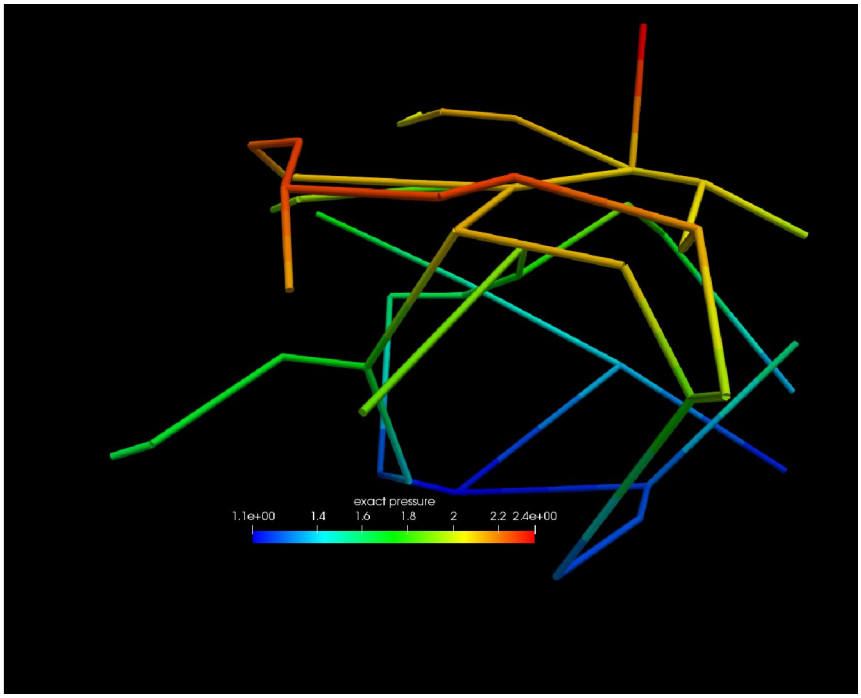

Figure 26: Pressure profile [Pa] in the 1D brain network

6.2 Computations of flow in a section of renal arterial network

The arterial vascular data provided by Nordsletten [8] has been converted in a Dune Grid Format (DGF), which is required by DumuX in order to run the simulations of flow and transport.

The simulations in the kidney are executed on the top of an example already developed in DumuX that concern a 1-dimensional network embedded in a 3-dimensional matrix. In particular, blood is flowing through the 1D network grid. The 1D network has been replaced with the 1D grid obtained from Nordsletten data, and the dimension of the 3D matrix were adjusted according to the sizes of the available renal vasculature. For both the 1D and 3D domain is considered an isothermal single-phase flow (1p-1p). The temperature is set to 37°C.

The vessel walls are treated as part of the tissue domain [17], thus, the permeability value is the same in both domains and in this example it is equal to one, as shown in Table 9. The tissue that surrounds the vasculature is represented as a homogeneous medium in the present work.

Spatial Parameters	
Tissue Permeability [m^2]	1.0
Vessel Permeability [m^2]	1.0

Table 9: Spatial Parameters of the renal arterial tree

Table 10 shows the boundary conditions set for the section of renal arterial network.

Boundary Conditions (1D)	
Pressure Input [Pa]	2.0
Delta Pressure [Pa]	1.0

Table 10: Boundary Conditions for the renal arterial tree

In the following, the pressure distribution in Pa and the velocity profile in cm/s obtained as results on the simulations of flow in the section of the renal arterial network are shown.

Figure 27 shows the pressure profile in part of the arterial 1D network, represented in Figure 19. In particular, it highlights that there is a pressure drop from inlet to outlet: the pressure decreases from 2.5 Pa in the inlet to 1.1 Pa in the outlet. This result is qualitatively correct because the pressure is higher in the renal artery, and then it decreases moving towards the smaller vessels, allowing blood to flow through the capillaries.

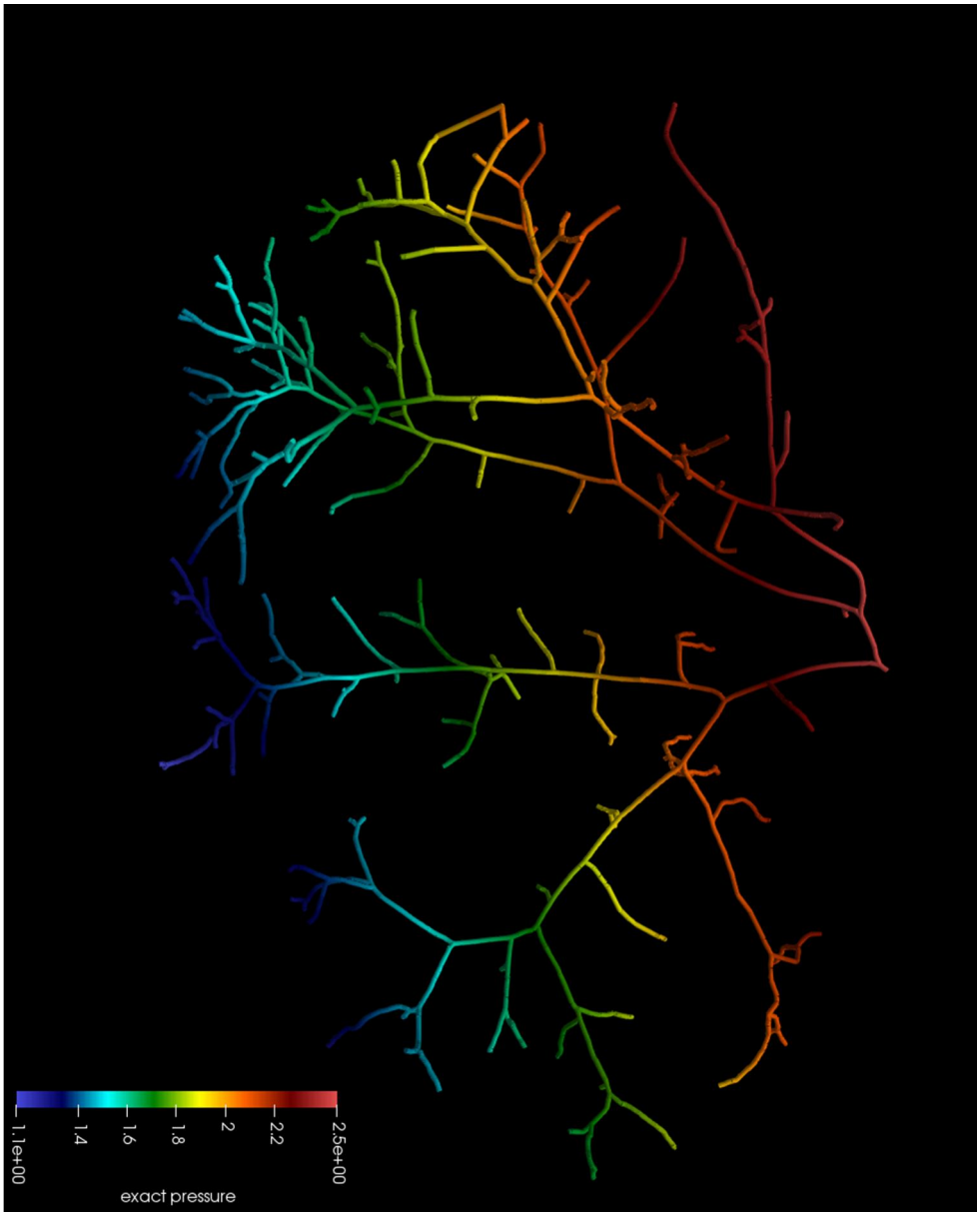

Figure 27: Pressure distribution [Pa] in the section of renal arteries 1D network

Figure 28 shows a qualitative representation of the pressure distribution [Pa] in the 1D network of the section of the renal arterial tree, embedded in the 3D domain. From Figure 28, it is possible to qualitatively notice the flow from the arteries to the surrounding tissue, where there is the presence of spots of higher pressure.

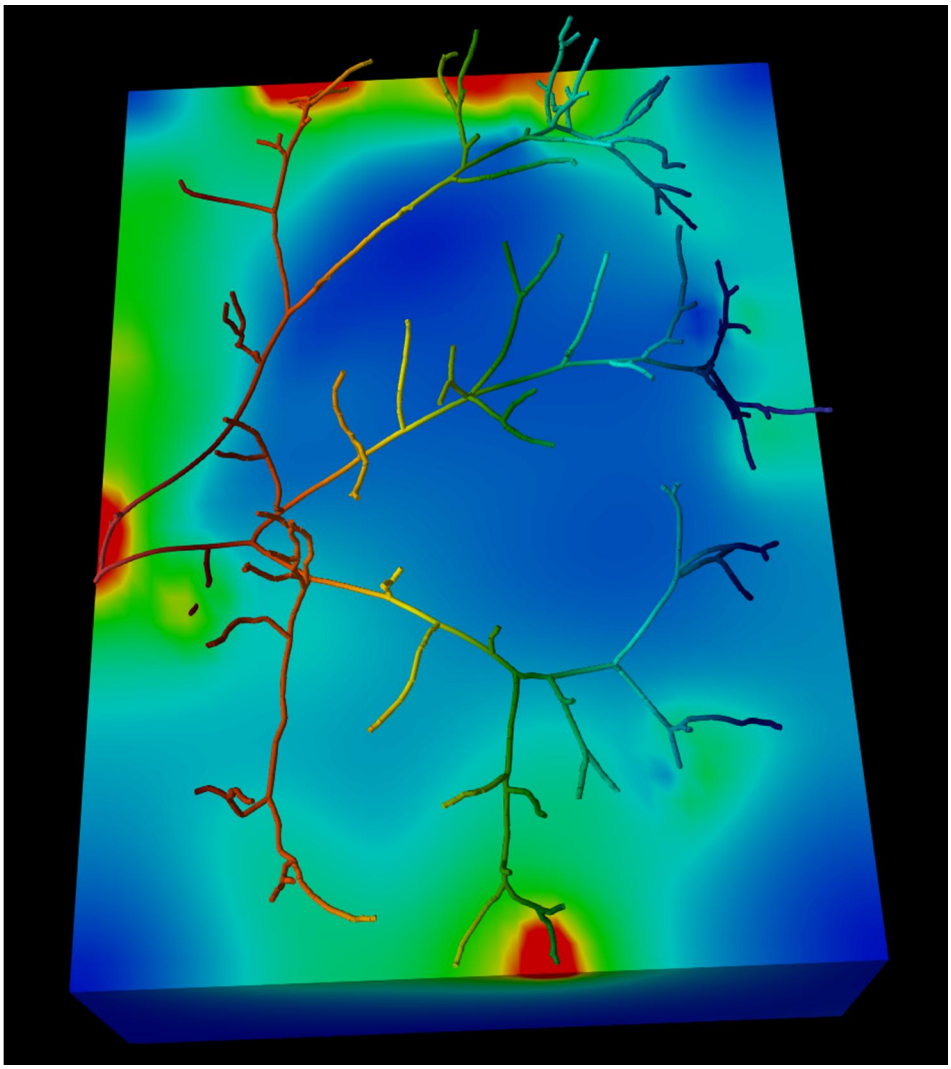

Figure 28: Pressure distribution [Pa] in the section of renal arterial tree embedded in the 3D domain

Figure 28 shows a preliminary and qualitative result since the venous tree is missing.

Figure 29 instead shows the blood velocity profile [m/s] in the section part of arterial tree.

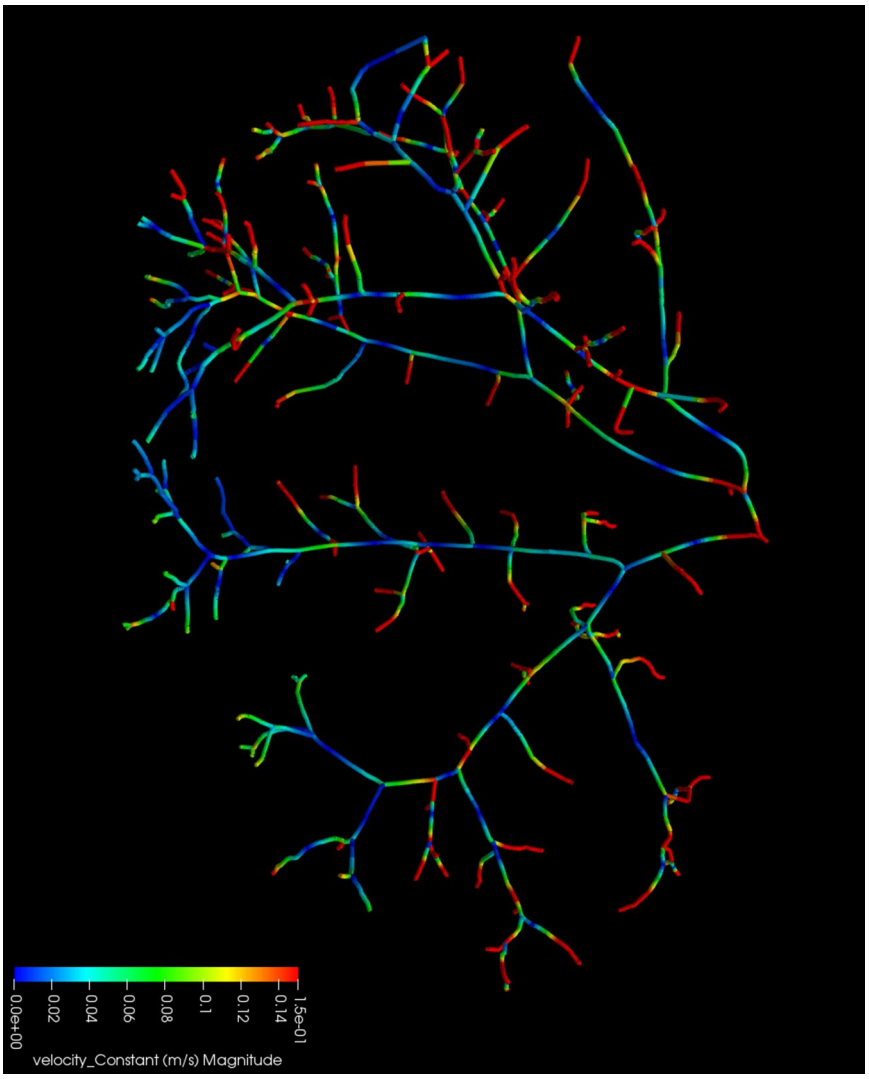

Figure 29: Velocity distribution [m/s] in the renal arteries 1D network of the section of renal arterial tree

The simulations of blood flow were not conducted in the renal venous tree. Thus, this computational modeling of flow in the kidney is a preliminary work because the venous tree is missing.

7. Summary and Conclusions

This thesis has studied flow in 1D realistic vascular networks, and their interaction with a surrounding 3D grid. In a physiological context, which is the primary intention of this thesis, this translates to supply of oxygen from blood vessels (1D network) to a 3D homogeneous tissue (3D space).

The first part of the thesis involved an understanding of renal anatomy and physiology and processing of anatomical data available from Nordsletten [8]. The second part involved studies of Stokes flow in the DumuX framework and qualitative studies thereon. While Kidney was the main background application, in the absence of further anatomical data we based our studies on microvascular networks of different organs as similar mathematical and computational concepts are usually applied for studies on different organs.

The main function of the kidneys is to filter blood, resulting in the removal of waste substances through the urine. They also contribute to the regulation of blood pressure and the concentration of red blood cells in the body, which are important factors in maintaining body homeostasis. Based on the detected oxygen concentration, the kidneys produce erythropoietin (EPO) which stimulates the production of erythrocytes. Inaccuracy in renal oxygen regulation can have consequences on the concentration of red blood cells and can thus lead to chronic kidney disease. The phenomenon of oxygen consumption in the kidneys is still not clear.

With the help of computational models based on high resolution synchrotron radiation-based imaging, the first aim of the thesis was to determine oxygen distribution in the kidney. The first part of the master project has involved an understanding of anatomy of the kidney accomplished in parallel with processing of the Nordsletten data [8] using software tools to obtain information about the renal vasculature. The obtained network has been then used for the simulations of flow and transport conducted on DumuX.

In parallel, and in addition to kidney, general methods for O2 transport in other organs, and in particular in microvasculature networks were explored while the renal data was being processed. Secomb et al. [17] have conducted simulations of oxygen transport to tissue and they made available their microvascular network structures of brain, cardiac tissue, skeletal muscle and tumor (*source: http://physiology.arizona.edu/people/secomb/network*). The available data of the microvascular networks has been converted in a DGF format in order to run the simulations of flow and transport on DumuX. In particular each 1D microvascular network is embedded in a 3D domain, representing the surrounding tissue. For both the 1D and 3D domain is considered a single-phase flow (1p-1p).

Before conducting the simulations of flow and transport of interest, obtaining a proper model of the vasculature from the medical images is essential. In the biomedical field image processing and in particular image segmentation are very important processes because they support physicians in the analysis and diagnosis of different diseases, in the study of anatomical structure of the organs and in the decision of the proper therapy. There has been an increase of CT images for the diagnosis and treatment of diseases, thus segmentation of human organs from this type of imaging is a necessary step when deciding the correct treatment. Kidney segmentation is a challenging work because the intensity values of the grey scale that characterize kidney are similar to those of the organs next to the kidney [19]. Furthermore, using X-ray micro-computed tomography, it is laborious to elucidate the full three-dimensional structure of the renal vasculature in its entirety down to the smallest capillaries.

At The Interface Group, X-ray micro-computed tomography (μCT) images of the kidney were available. However, the data was huge and the segmentation of the vessels was not achievable only through VMTK. The image processing would have been challenging and time consuming, and for these reasons, the available kidney images were not taken in to account for this thesis.

7.1 Processing of Available Renal Vascular Data

A renal vasculature model was needed in order to study flow and transport in the kidney. Nordsletten et al. [8] made available data on renal vasculature, obtained from an automatic segmentation technique applied to micro-computer tomography images acquired from a rat.

The vascular data of the venous and arterial tree was processed on the graphical user interface CMGUI, an advanced 3D visualisation software package with modelling capabilities. The first objective was to reconstruct a 3D geometry from the network provided by Nordsletten. Thanks to CMGUI it was possible to reconstruct the surface of the vessels using *cylinders* as graphical representation, and considering the radius values detected by Nordsletten. From the Graphics Window of CMGUI it was visualized the reconstructed vessel and it was possible to state that it presented gaps where cylinders should have merged, thus it has been applied a smoothing process that refined the surface.

The obtained surface was saved in a STL format and then imported in Paraview to analyse more in deep the geometry. It has been noticed that inside the reconstructed vessel there were many artefacts, in particular at the bifurcations and where there is a tightening of the vessel. This might be related to the quality of the mesh, i.e. there are neighbouring elements that differs in size and the bifurcations have a single derivative. In order to fix this problem, it has been tried to remove manually the artefacts with the help of Blender, a 3D computer graphics software. This approach was however not successful, thus the 1D network has been adopted.

The studies of flow and transport in the renal vascular model provided by Nordsletten were conducted on DumuX, DUNE for Multi-{Phase, Component, Scale, Physics, ...} flow and transport in porous media. In particular, the available data was converted in a DGF format, which is required by DumuX in order to execute the simulations.

The 1D vascular network was embedded in a 3D domain representing a porous tissue. For both the 1D and 3D domain was considered a single-phase flow (1p-1p) governed by the Darcy's law. The results focus on the pressure and velocity profile in the vascular network and in the surrounding tissue.

7.2 Transport and Consumption of Oxygen in the Kidney

Living organisms require continual free energy for carrying out activities. Energy is generated in the form of adenosine triphosphate (ATP). Oxygen is one of the main component for the energy production within the cells. It is provided to the body by breathing. After diffusing from the lung into the red blood cells, O2 binds to hemoglobin. O2 transported in the arterial blood is then diffused to the tissues where it is consumed for production of ATP.

Oxygen homeostasis is crucial for the right functioning of the body. It depends on both the respiratory and cardiovascular systems. It also depends on the capacity of the blood to transport the oxygen, which is related on the amount of hemoglobin in the blood. When there is a reduction of oxygen concentration in the arteries, renal fibroblasts deliver erythropoietin, an erythropoiesis stimulator. At the contrary to the respiratory and cardiovascular systems, the response of kidneys takes time to have effect.

Thus, the kidneys play a key role in oxygen homeostasis by controlling the production of red blood cells. This control is achieved through the delivery of the hematopoietic growth factor EPO, produced by the kidneys as a reaction to two main stimuli: reduction in the capacity of blood to carry Oxygen (anaemic hypoxia) and reduction in arterial oxygen tensions (hypoxic hypoxia) [3].

The kidney consumes oxygen principally to produce energy for tubular reabsorption. Relative to the kidney's request for oxygen, the renal blood flow (RBF) is normally high, thus the kidney takes out only a small portion of the oxygen they receive [20]. The corticomedullary gradient of oxygen is clarified by the combination of vessels in the medulla: the tubules and vessels of the medulla are arranged in a hairpin loop pattern to permit countercurrent transfer of solutes between the descending and ascending limbs, a system that allows adequate concentration of the urine. Because of this pattern, oxygen diffuses straight from the arterial to the venous branches of the vasa recta, decreasing oxygen supply to the deeper areas of the renal medulla. The medullary thick ascending limbs of Henle's loop has a fundamental function in this direction: active transport of NaCl in this duct is accountable for the production of an osmotic gradient in the

medulla, thus this process necessitates high energy. As a result of this, there is an important decrease of oxygen supply in the deeper areas of the renal medulla, near the medullary thick ascending limbs and far from the vasa recta [19].

However, the dynamics of renal oxygenation is poorly understood at date. Olgac and Kurtcuoglu [13] suggest that "cortical tissue oxygenation is determined mainly by the interaction between oxygen perfusion and consumption in the tissue, but not by the arterial-to-vein (AV) shunting in the preglomerular vasculature". They also show that oxygen is supplied to the tissue mainly by the preglomerular vasculature when oxygen consumption in the cortex is high or under hyperoxemic conditions. On the contrary, when the concentration of oxygen in the tissue is low, capillaries are the main source of oxygen.

7.3 Difference between Brain and Kidney O2 Consumption

To perform the normal functions necessary for survival, the brain uses about 20% oxygen. For this reason, the regulation of blood flow and oxygen transport is of fundamental importance. Because the brain requires a large amount of oxygen compared to other organs, acute hypoxia produces an increase in blood flow to the brain. Generally, blood flow does not change in the brain until tissue oxygen partial pressure (Po_2) drops below 50 mmHg, value below which cerebral blood flow largely increases. Increments in cerebral blood flow do not alters metabolism, but hemoglobin saturation decreases from 100% at Po_2 >70 mmHg to 50% at Po_2 <50 mmHg [22]. Acute hypoxia provokes an increase in cerebral blood flow through effects on vascular cells of cerebral arteries and arterioles.

The local Po_2 measurements within brain and kidney presented by Lübbers [23] demonstrated that "the heterogeneity of tissue Po_2 is large and similar in both organs". Since the heterogeneity is caused by the laws of diffusion that determine the oxygen transport in a perfused tissue, differences can be found only if a distinctive structure or a special metabolic situation occurs, as in the renal medulla.

Relative to its size, the kidneys receive a large amount of blood, about 25% of cardiac output. A portion of plasma is filtered and enters the nephron. A great portion of the filtrate in then reabsorbed. To carry on the process of reabsorption, the kidneys demand for a high quantity of energy. Indeed, although the human kidneys constitute a very small percentage of body, they employ 10% of the oxygen used in cellular respiration. Much of the oxygen consumed by the kidney is used to support the active reabsorption of Na+, principally along the proximal tubule and thick ascending limb. The supply of O2 to the renal medulla barely exceeds its O2 utilization, as illustrated in Table 11. The inhomogeneity of oxygen supply that characterizes the kidney has important implications for renal pathophysiology and disease [24].

Region or organ	O_2 delivery	Blood flow rate	O_2 consumption	O_2 consumption/ O_2 delivery
	ml/min/100 g			%
Hepato-portal	11.6	58	2.2	18
Kidney	84.0	420	6.8	8
Outer medulla	7.6	190	6.0	79
Brain	10.8	54	3.7	34
Skin	2.6	13	0.38	15
Skeletal muscle	0.5	2.7	0.18	34
Heart	16.8	84	11.0	65

Table 11: Comparison of the ratio of oxygen consumption to oxygen delivery in the outer medulla of the kidney to that of other organs [21]

Table 11 shows also the main difference between brain and kidney oxygen supply/consumption: considering the outer medulla, almost the 80% of the delivered O2 is then consumed in order to generate potential energy for tubular reabsorption. While the brain consumes 34% of the O2 delivery.

7.4 Future Work

In the United States the predominance of end-stage renal disease (ESRD) impact over 600000 patients that are being treated. ESRD is the terminal phase of chronic kidney disease (CKD). A large evidence indicating that CKD is caused by renal tissue hypoxia has led to the increase of therapeutic strategies that increment kidney oxygenation and the assertion that chronic hypoxia is the final path to end-stage renal failure [24].

In this direction, future work may focus on the obtaining of distribution of oxygen in the whole kidney, giving particular attention to the microvasculature, where O2 is mainly consumed due to the reabsorption process. In order to study flow and transport in the renal microvasculature a high resolution and precision representation of the capillaries and the nephron are needed.

For this reason, The Interface Group is working on high quality segmentation of blood vessels obtained from Synchrotron radiation-based images. After a challenging work on the image processing and image segmentation, it will be possible to study the flow and transport in the microvasculature of the kidney, focusing on the oxygen distribution within the nephron. Indeed, for a detailed understanding, full 3D computations should be performed.

Firstly, to improve the present work, also the renal venous tree should be involved. In this way, it is possible to consider the whole system consisting of macrovasculature (renal arterial and venous tree) and porous media, due to the lack of data on the microvasculature.

Moreover, the simulations on the renal vasculature 1D network conducted on DumuX can be improved by adopting complex mathematical model on the oxygen consumption in the kidney. For example the model used by Gardiner et al [12] or the mathematical model suggested by Olgac and Kurtcuoglu [13] could be implemented on DumuX in order to obtain more specific results on oxygen distribution within the kidney.

Another extension of the present work is to adopt on DumuX a single-phase 2-components (1p2c) model, instead of single-phase single-component, for simulating both solute transport and oxygen consumption along the nephrons. This would allow studying for example how the reabsorption of Na+ in the glomerulus and O2 consumption are correlated: much of the oxygen consumed by the kidney is consumed to support the active reabsorption of Na+, principally along the proximal tubule and thick ascending limb of the nephron. Softwares like DumuX should be developed and enhanced, and made open source for use by public, so that software engineering principles are followed in scientific software development.

Considering together all the future developments afore mentioned, it is possible to obtain a fulfilling project that may help and assist physicians in making treatment planning or prevention for kidney diseases.

Bibliography

[1] “Kidney NCCR,” [Online]. Available: https://kidneynccr.bio-med.ch/cms/.

[2] N. Kleinstreuer, *"Mathematical Modeling of Renal Autoregulation",* 2009.

[3] K. Eckardt, “Distribution of erythropoietin producing cells in rat kidneys during hypoxic hypoxia,” *Kidney International,* pp. 815-823, 1993.

[4] P. Maxwell, «Identification of the renal erythropoietin-producing cells using transgenic mice,» *Kidney International,* pp. 1149-1162, 1993.

[5] M. Le Hir, «Structure-function correlations in erythropoietin formation and oxygen sensing in the kidney,» *Klin Wochenschr ,* pp. 567-575 , 1991.

[6] K. M. Erbertseder, *"A Multi-Scale Model for Describing Cancer-Therapeutic Transport in the Human Lung",* 2012.

[7] J. Bear, Dynamics of Fluids in Porous Media, Courier Corporation, 1972.

[8] D. A. Nordsletten, «Structural morphology of renal vasculature,» *Am J Physiol Heart Circ Physiol,* 2006.

[9] A. N. Strahler, «Hypsometric (Area Altitude) Analysis of Erosional Topology,» *Geological Society of America Bulletin,* pp. 1117-1142, 1952.

[10] «CMGUI or Continuum Mechanics Graphical User Interface,» [Online]. Available: http://www.bioeng.auckland.ac.nz.

[11] R. Evans, «Intrarenal oxygenation. unique challenges and the biophysical basis of homeostasis,» *Am J Physiol Renak Physiol,* pp. 1259-1270, 2008.

[12] B. Gardiner, «A mathematical model of diffusional shunting of oxygen from arteries to veins in the kidney,» *Am J Physiol Renal Physiol,* pp. 1339-1352, 2011.

[13] U. Olgac e V. Kurtcuoglu, «Renal oxygenation: preglomerular vasculature is an unlikely contributor to renal oxygen shunting,» *Am J Physiol Renal Physiol,* pp. 671-688, 2014.

[14] «DUNE,» [Online]. Available: http://www.dune-project.org.

[15] B. Flemisch, *DuMux: DUNE for Multi-{Phase, Component, Scale, Physics, ...} Flow and Transport in Porous Media,* Stuttgart, 2010.

[16] «Dumux,» [Online]. Available: http://www.dumux.org/documents/dumux-handbook-2.11.pdf.

[17] T. W. Secomb e R. Hsu, «Green's Function Methods for Analysis of Oxygen Delivery to Tissue by Microvascular Networks,» *Annals of Biomedical Engineering,* vol. 32, n. 11, p. 1519–1529, 2004.

[18] H. Song, «Kidney segmentation in CT sequences using SKFCM and improved GrowCut algorithm,» in *IEEE International Conference on Bioinformatics and Biomedicine*, Belfast, 2014.

[19] A. Deng, «Kidney oxygen consumption, carbonic anhydrase, and proton secretion,» *Am J Physiol Renal Physiol,* p. F1009 –F1015, 2005.

[20] F. H. EPSTEIN, «Oxygen and renal metabolism,» *Kidney International,* vol. 51, p. 81—385, 1997.

[21] M. Cipolla, The Cerebral Circulation, San Rafael (CA): Morgan & Claypool Life Sciences, 2009.

[22] D. W. Lubbers, «Heterogeneities and profiles of oxygen pressure in brain and kidney as examples of the PO2 distribution in the living tissue,» *Kidney International,* vol. 51, p. 372—380, 1997.

[23] Q. Fu, «Hypoxia: The Force that Drives Chronic Kidney Disease,» *Clinical Medicine & Research,* vol. 14, n. 1, pp. 15-39, 2016.

[24] P. Hansell e W. J. Welch, «Determinants of kidney oxygen consumption and their relationship to tissue oxygen tension in diabetes and hypertension,» *Clin Exp Pharmacol Physiol,* p. 123–137, 2013.

[25] T. Secomb e R. Hsu, «Simulation of O2 transport in skeletal muscle: diffusive exchange between arterioles and capillaries,» *Am. J. Physiol,* pp. 1214-1221, 1994.